Conceptual Model of Menengai geothermal prospect: an update from new Audio Magnetotellurics, Magnetotellurics and Transient Electromagnetic data

Daniel Samperu Saitet

A thesis submitted in partial fulfillment for the degree of Master of Science in Physics in the Jomo Kenyatta University of Agriculture and Technology

2012

DECLARATION

This thesis is my original work and has not been presented for a degree in any other University.

Signature: ……………………………   Date: ……………………………..

Daniel Samperu Saitet

This thesis has been submitted for examination with our approval as University Supervisors:

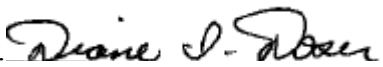Signature: ……………………………   Date: ……………………………..

Dr. Maurice K'orowe

JKUAT, Kenya.

Signature: ……………………………   Date: …………………………………

Dr. Nicholas Mariita

KenGen, Kenya.

Signature: …~~Diane J-Doser~~   Date: …………………………………

Prof. Diane Doser

University of Texas at El Paso, USA.

DEDICATION

This work is dedicated to those who carry lanterns deep into the darkness to search for these metals. They dig tunnels in distant, unknown places, where they dangle by ropes. Far beneath the grain fields, fires are built to break loose those rocks that have jewels of gold. They go to places unseen by the eyes of hawks; they walk on soil unknown to the proudest lions. With their own hands they remove sharp rocks and uproot mountains. They dig through the rocks in search of jewels and precious metals. They also uncover the sources of rivers and discover secret places.

ACKNOWLEDGEMENT

TABLE OF CONTENTS

LIST OF FIGURES

x

LIST OF APPENDICES

LIST OF ABBREVIATIONS

2D   Two dimensional

3D   Three dimensional

AMT   Audio Magnetotellurics

CO$_2$ Carbon Dioxide

EDI   Electronic Data Interchange

GI   Geotermica Italiana

H$_2$S   Hydrogen Sulphide

KHz   Kilo-Hertz

KRISP   Kenya Rift International Seismic Project

MT   Magnetotellurics

TEM   Transient Electromagnetic

TVA   Tectono-volcanic Axis

UNU-GTP   United Nations University-Geothermal Training Program

ABSTRACT

This study involved collection and analysis of resistivity data using Transient Electromagnetic (TEM), Magnetotellurics (MT) and Audio Magnetotellurics (AMT) techniques in the area within and surrounding the Menengai caldera of central Kenya. Both AMT and MT data were corrected for static shift using TEM data from stations in their proximity and an integrated data set is obtained. Data collected previously in the same area using these techniques was also incorporated into the working data base. Inversion of these data sets was performed using the WinGlink Interpretation software. Using this integrated data base, resistivity contour maps were plotted for the Occam inversion at different elevations. Two-dimensional resistivity models were generated using four profiles cutting across the caldera. Interpretation of these results shows three areas with possible exploitable geothermal resources; the Western sector extending about 5km southwesterly, the central caldera region and the southern region. A conceptual model was developed for the Manengai geothermal field. The experience of Olkaria geothermal power density is extrapolated to estimate the potential power generating capacity of the Menengai geothermal field. It is concluded that the resource available at Menengai is sufficient to sustain a steam power generation plant of not less than 836 MW of electricity for a steady production period of 25 years.

CHAPTER ONE

1.0 INTRODUCTION

1.1 Overview

The Kenyan government has identified geothermal resources as the solution to the common power crisis observed in the country for the better part of the last decade (Kiva, 2009). Frequent droughts and rising costs of petroleum products have forced the government to review its policy on energy. Moreover, the destruction of forests and other catchment areas have already demonstrated their effects on the climate and hence reliance on hydroelectricity alone is no longer an option. There is therefore a need to develop clean and environmentally benign alternative sources of energy. The Kenyan government recently constituted a task force on accelerated development of green energy with a target of developing an extra 2000MW of electricity from renewable resources, most of which will come from geothermal sources by mid-year 2012 (Kenya Gazette - CXI - No. 54 - 19th June 2009).

Geophysical methods have a significant role in the investigation of geothermal prospects because they provide the means of finding deep sub-surface structures without drilling. The choice of a particular method to apply depends on the objective, the type of the geothermal prospect and the cost of the survey. The geophysical techniques that have been previously used in geothermal energy exploration in Kenya's rift valley include direct current (DC) resistivity, gravity, transient electro-magnetic and magnetotellurics.

The rocks within the earth's subsurface have many physical properties that vary from place to place. The common properties include electrical conductivity, magnetic susceptibility, density contrasts and seismic wave velocities. Geophysics is the science that studies the variation of any of the above mentioned properties across the surface of the earth. If the measured property over an area is different from that of the surrounding regions, it is referred to as anomalous.

1.2 Characteristics of a Geothermal System

Geothermal resources occur under certain physical and structural conditions. The three major characteristics of such systems are listed below:

- *The heat source* - ordinarily this would be a magmatic body at very high temperature.

- *Reservoir*- is a highly fractured region that allows deep fluid circulation. It should allow for conduits for the fluid to pass through. A typical reservoir has a cap formed of impermeable rock that traps the fluid under pressure. The reservoir may either be liquid/water dominated or steam dominated.

- *Recharge* – a good geothermal system includes a source of fresh (cold) water to recharge the water being diminished by escaping steam. Apart from a source, there should be pathways for the liquid to percolate into the hot region.

Figure 1.1 shows a generalized conceptual model showing the components of a geothermal system. The development of a conceptual model helps when developers of geothermal energy utilization projects are planning or exploiting the resources. Figure 1.2 is one such attempt at developing a conceptual model for the Menengai prospect.
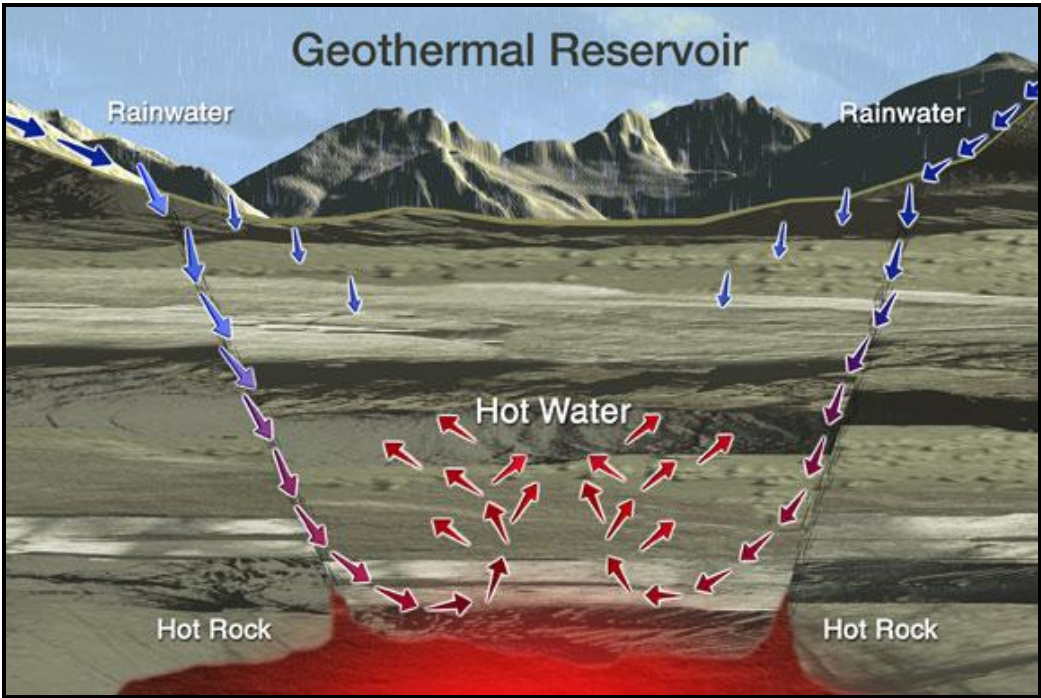
Figure 1.1 A conceptual animation of a generalized geothermal system (UNU-GTP/KenGen, 2008)
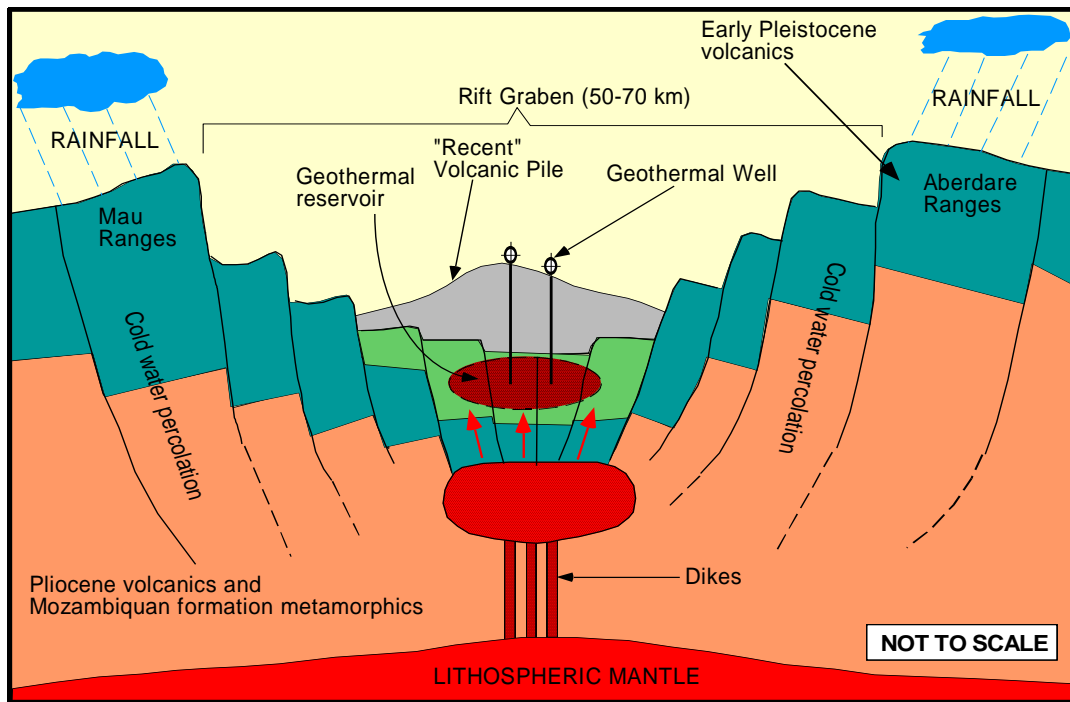
Figure 1.2 A typical model of a geothermal system in the Kenyan rift (UNU-GTP/KenGen, 2008)

1.3 Geological and Tectonic Setting

Menengai is a relatively seismically active area located in the region where the failed Kavirondo rift branch joins the main Kenyan rift. Two rift floor tectono -volcanic axes (Molo and Solai) terminate at Menengai (KenGen, 2004). Figure 1.3 shows the tectonic and structural setting of Menengai with respect to the main Kenyan rift

Menengai volcano is probably of Pliocene age and consists of a collapsed caldera covering an area of approximately 70 km^2 (McCall, 1967). The caldera floor is composed of panteliric trachytes with a ring of Menengai tuff covering most of the area from the west side going from south to the north east side. Shield trachytes are observed

4

further south. The caldera is superimposed on an area dominated by pyroclastics extending to the Olrongai and Olobanita volcanic centres. Figure 1.3 displays the caldera in relation to the two TVA's and the rift fault. Figure 1.4 shows a geological map of the Menengai region and the surrounding areas (KenGen, 2004).
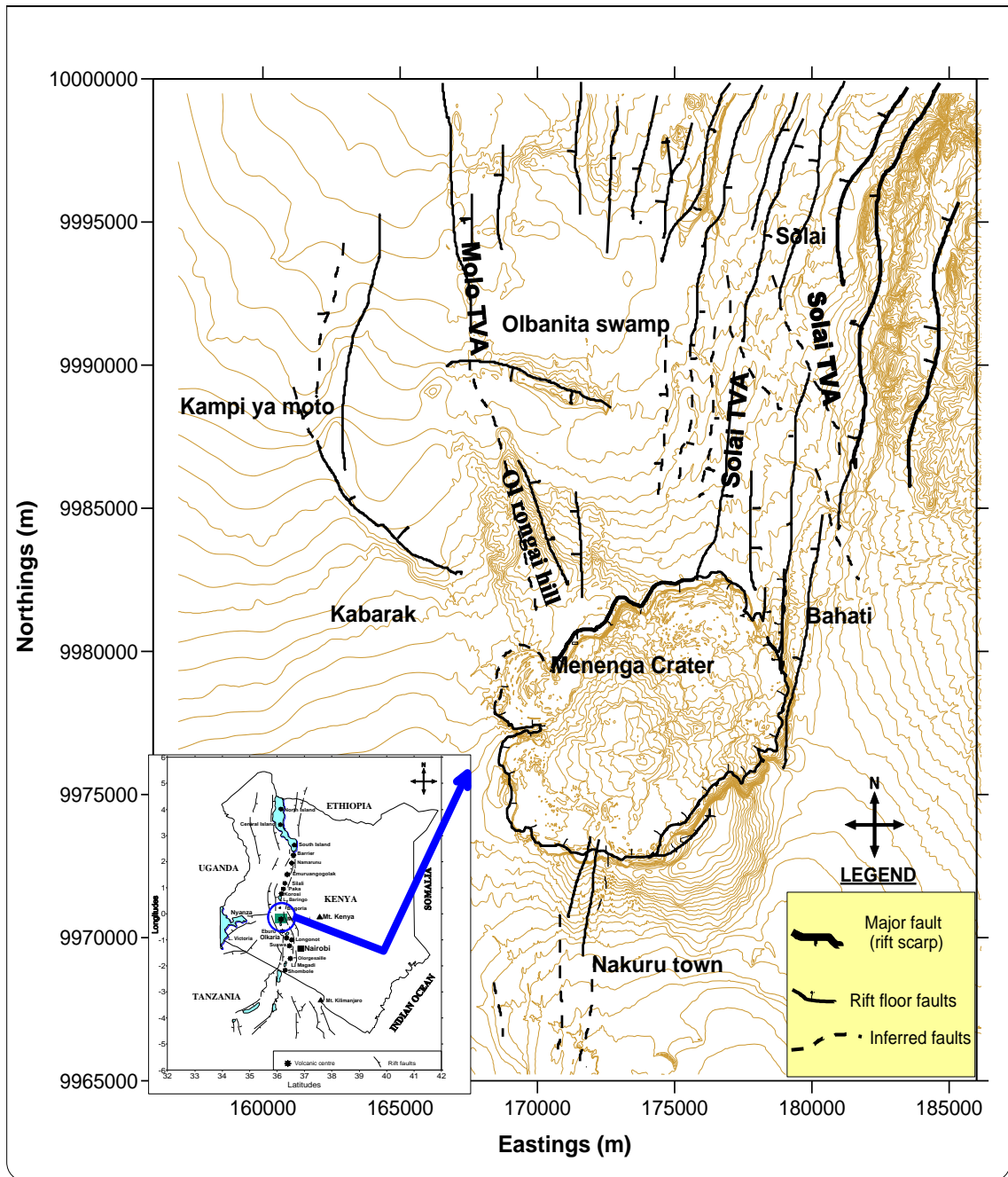
Figure 1.3 A structural map of Menengai showing its location at the intersection of two major tectono-volcanic axes and elevation contours. Inset is the map of Kenya showing the location of Menengai.
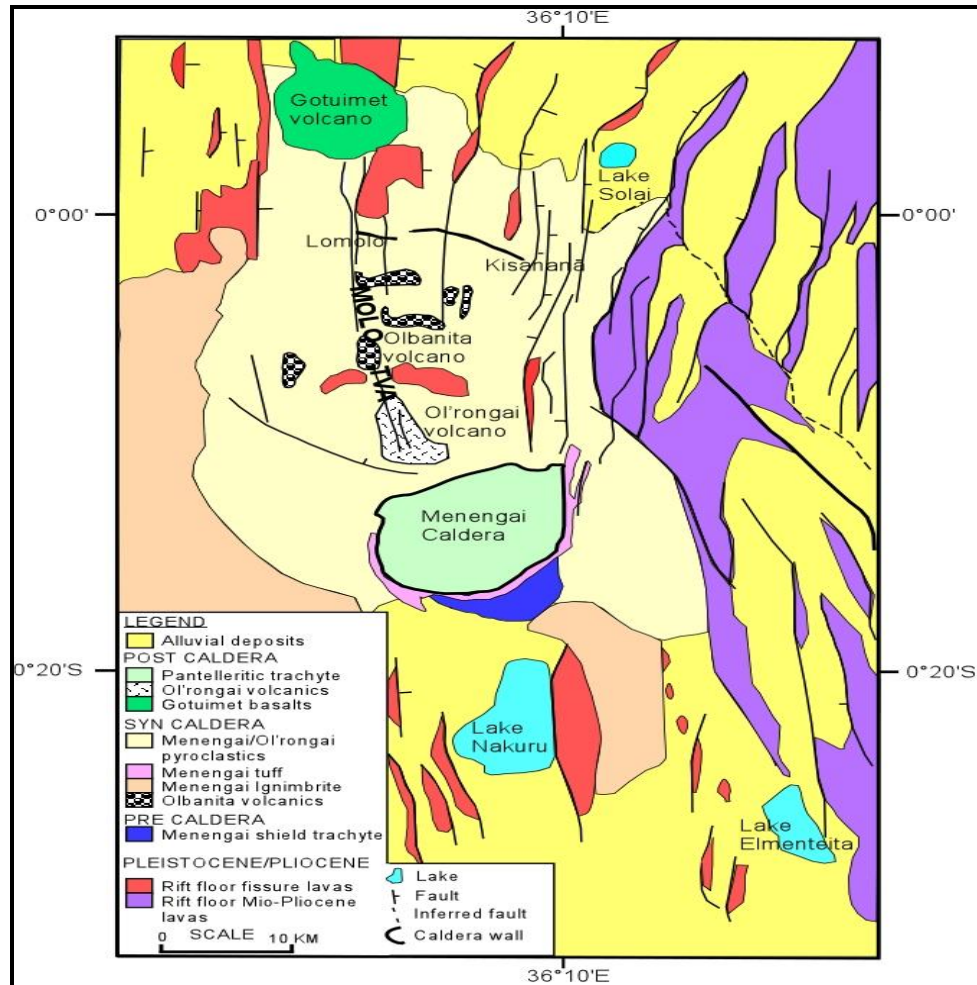
Figure 1.4 A geological map of Menengai and its environs.

1.4 Statement of the Problem

Previous geophysical studies at Menengai did not adequately cover the area within the caldera. The major reasons were that the caldera floor was perceived as a volcanic risk and the difficult terrain in the area made it inaccessible. More recent surveys involved data collection in part of the caldera but there were still large data gaps for a conclusive delineation of geothermal resources in the prospect. There was therefore need for

collection of infill data to reasonably understand the resistivity structure beneath the prospect area.

The techniques used in prior studies were to a large extent DC resistivity method with some enhancement using MT methods. The DC resistivity methods could not penetrate to sufficient depths especially due to the limitation on the length of the loop and presence of resistive lava piles near the surface. MT studies suffer static shift problems which in this study were corrected by carrying out TEM soundings.

The MT method is more reliable in mapping deeper levels and hence the need to understand the shallow resistivity structure as well. With advancement in technologies, the AMT equipment has recently been acquired by KenGen. A combination of MT and AMT is expected to resolve the resistivity structure from shallow depths to deeper levels.

Most studies so far done at Menengai were aimed at delineating anomalies and few attempts were made to develop a conceptual method for the prospect. With a more complete data set, the available conceptual model need be updated.

1.5 Objectives

1.5.1 General Objective

To update the conceptual model of the Menengai geothermal system based on new resistivity data

1.5.2 Specific Objectives

i)   Develop an integrated Audio Magnetotelluric (AMT), Magnetotelluric (MT) and Transient Electomagnetic (TEM) model of the Menengai geothermal system

ii)   Quantitatively deduce the extent of the geothermal resources in the prospect

1.6 Justification

The Magnetotellurics method is based on induced electromagnetic fields whose sources are outside the earth and therefore are not affected by terrain and electrode polarization, as is the case for DC methods. This methodology is expected to overcome these challenges experiences by DC methods. Through their use of a wide range of frequencies they are capable of probing the subsurface from shallow to much deeper levels. The use of Audio Magnetotellurics alongside ordinary Magnetotellurics techniques aids in enhancing the integrity of near surface resistivity structure.

The acquisition of additional data within the caldera will improve the existing datasets for better analysis and interpretation of the resistivity structure. This aids in the development of a more data constrained model of the subsurface to addition to existing datasets.

With better resistivity maps and cross sections, the components of the system and their characteristics may be understood. These results will locate the upflow and inflow zones

and estimate expected temperature distributions to aid future developers in locating sites

for production and reinjection wells.

CHAPTER TWO

2.0 LITERATURE REVIEW

Previous geoscientific studies carried out in the Menengai area for geothermal energy (Geotermica Italiana, 1987; KenGen, 2004) suggested that there is preferential magma upwelling at Menengai that may be associated with thermal anomalies in the area. The area is also endowed with appreciable volumes of permeable rocks created by recent extensional faulting at depth, which may be potential reservoirs.

Menengai shows other surface manifestations of a geothermal system. First, there is a collapsed caldera which is a very strong signal for an occurrence, at least at some time, of a magmatic upwelling. But the question of whether the system is still active is verified by the presence of fumaroles, hot water boreholes, geothermal related vegetation and high counts of CO_2, H_2S and radon gas. Fumaroles are mainly located within the caldera floor, whereas hot water boreholes with CO_2 emanating from them are mainly found in the Ol'rongai and along a zone that extends northwestwards between Kampi ya Moto and Olbanita. In localities towards the northwest limit of the prospect, shallow boreholes meant for domestic water show anomalous thermal characteristics with three of them producing low pressure steam and one hot water at 98°C (KenGen, 2008).

Geotermica Italiana (1987), under the auspices of United Nations/Government of Kenya project KEN/82/002, carried out resistivity studies in the Menengai geothermal prospect area aimed at providing data for interpretation of the geothermal system. The Menengai

caldera floor was avoided due to its rugged terrain as well as being seen as a 'volcanic risk', so no data were collected within and around the caldera. The resistivity survey identified three broad areas thought suitable for further evaluation by exploration drilling (see Figure 2.1).

(1) The central area with a thick heterogeneous first layer (>1000 m), that lies above a resistive basement (>100 Ωm). This area has intermediate to high resistivity and covers the Ol'rongai and Olbanita area where steaming and dry hot wells are located.

(2) The western domain is separated from the central one by a structural discontinuity. This zone has a thick (1000-1500 m) homogenous electrical response and low resistivity (<10 Ωm). The conductive layer is above a resistive basement of >80 Ωm which corresponds to volcanics exposed on the rift flanks. The low resistivity was attributed to lithology rather than alteration.

(3) The eastern zone has resistivities similar to those of the western zone. However, the top of the resistive basement is shallower (1000-1200 m). The low resistivity was attributed to intense hydrothermal alteration.

In 1998, KenGen re-interpretation of all previous resistivity data and their results confirmed the earlier findings by Geotermica Italiana (1987). Results of these study were presented in KenGen, 2008 where a distinct low resistivity anomaly (<15 Ωm) was shown to occur to the west of the Menengai crater and the western anomaly extends into the Ol'rongai estate to the NW of Menengai in the Solai-Kisanana areas shown in figure

2.1. At 1000 m.a.s.l. the three distinct areas previously identified by Geotermica Italiana were clearly seen.
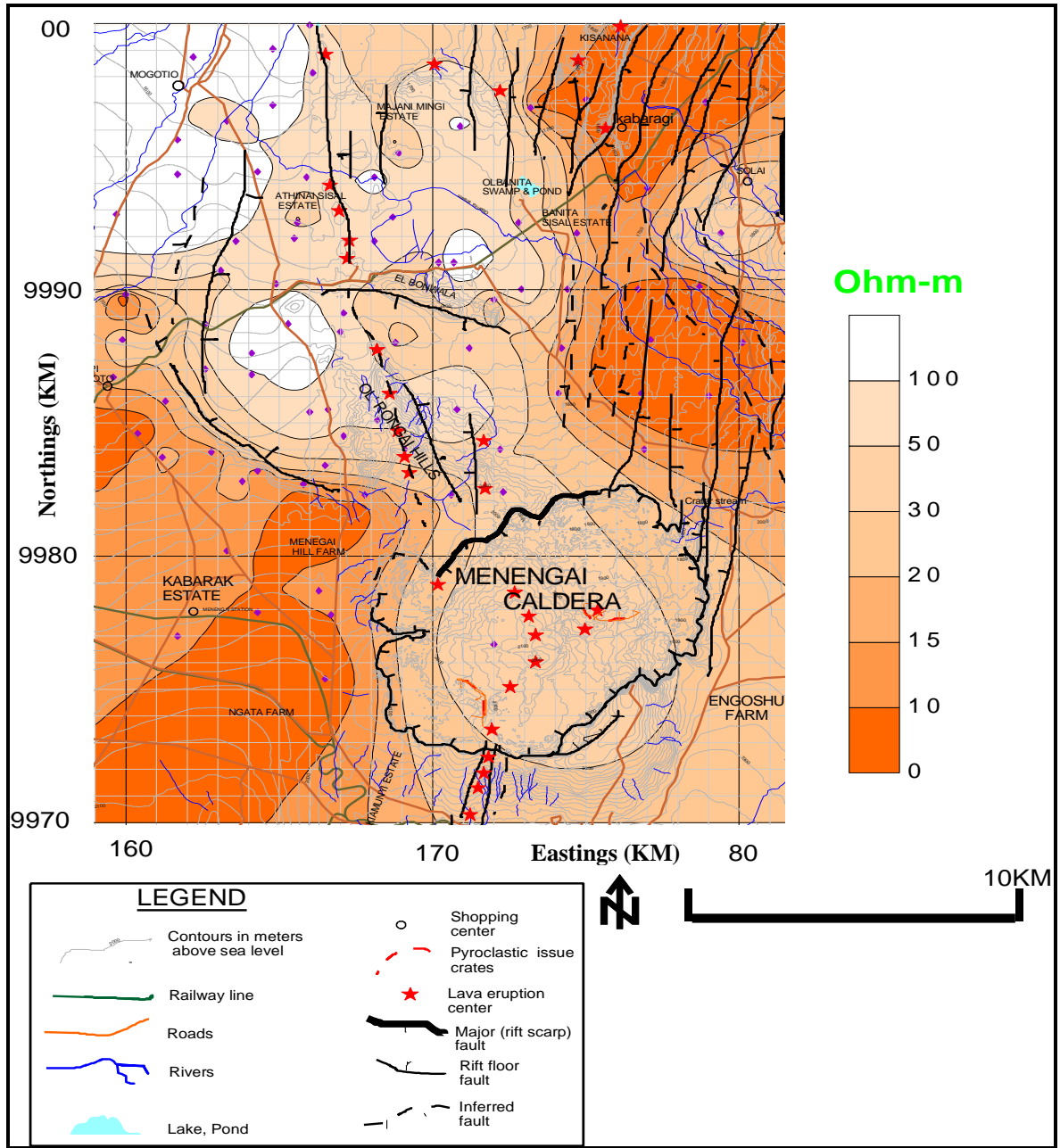
Figure 2.1 Resistivity distribution at 1000 m.a.s.l. in the Menengai area. Prepared by
Kengen from the Geotermica Italiana (1987) Schlumberger data. The diamonds in the
figure show location of data collection sites.

Geotermica Italiana (1987) carried out gravity surveys collecting data from 1400 stations. Analysis of these data showed a large positive anomaly located in the central part of the area. They interpreted this anomaly to be related to a dense body located some 3½ - 4 km deep with a density of 2.8 gcm^{-3} that could be interpreted as a heat source for the geothermal system. This anomaly coincides with the Molo Volcanic Axis as displayed in Figure 2.2.Data from the Solai area showed that the N-S trending anomaly, which reaches a maximum in the Molo Volcanic Axis, is less prominent within the Solai fault zone. Despite the Solai fault zone having relatively intense tectonic activity, it is less volcanically active than the Molo axis system with relatively few eruptions of lavas. The conclusions from this study showed that although there was high tectonic activity, there was no evidence for the existence of a localized heat source making it less attractive as a prospect. Similarly, based on the gravity data, the Menengai caldera area was given a low priority because of its terrain and perceived volcanic hazards.

Gravity data interpreted by Kenya Rift International Seismic Project (KRISP) (Simiyu and Keller, 1997) along a regional profile that runs across Menengai show a gravity high with an amplitude of 40 mgal and an EW wavelength of 35 km. This anomaly was modelled as an intrusive body about 13 km wide and extending to within 4 km depth of the surface as shown in Figure 2.3. Mariita (2003) carried out filtering analysis of the gravity data from the area and found that as the wavelength of the filter pass band was increased the wavelengths and amplitudes of the anomalies changed, implying deeper roots for the causative structures. The individual gravity highs of Ol'rongai and Olbanita

volcanic centres and Menengai caldera merge, giving the impression of a continuous gravity high along the Molo TVA.

Recent gravity and seismic studies of the Menengai area whose results are displayed as figure 2.4 identified bodies suspected to be magma chambers that could constitute the heat sources located directly beneath the caldera (Simiyu and Keller, 1997; 2001). Resistivity investigations revealed anomalies in areas north of the caldera (Geotermica Italiana, 1987). On the basis of these previous surface exploration activities at Menengai geothermal prospect, three sites were proposed for exploration wells. These were located on the geological structures where vertical permeability was expected.

Recommendations from these previous studies were that further work needed to be done, including full coverage of the prospect area with resistivity data collection stations. With this data it was envisaged that the extent, geometry and nature of the geothermal system would be better understood. This study focuses on the area identified as a plausible prospect where more data are collected and integrated with existing data sets and are jointly interpreted. The conceptual model of the prospect was constructed with constraints from inferences from the complete data set available for Menengai.
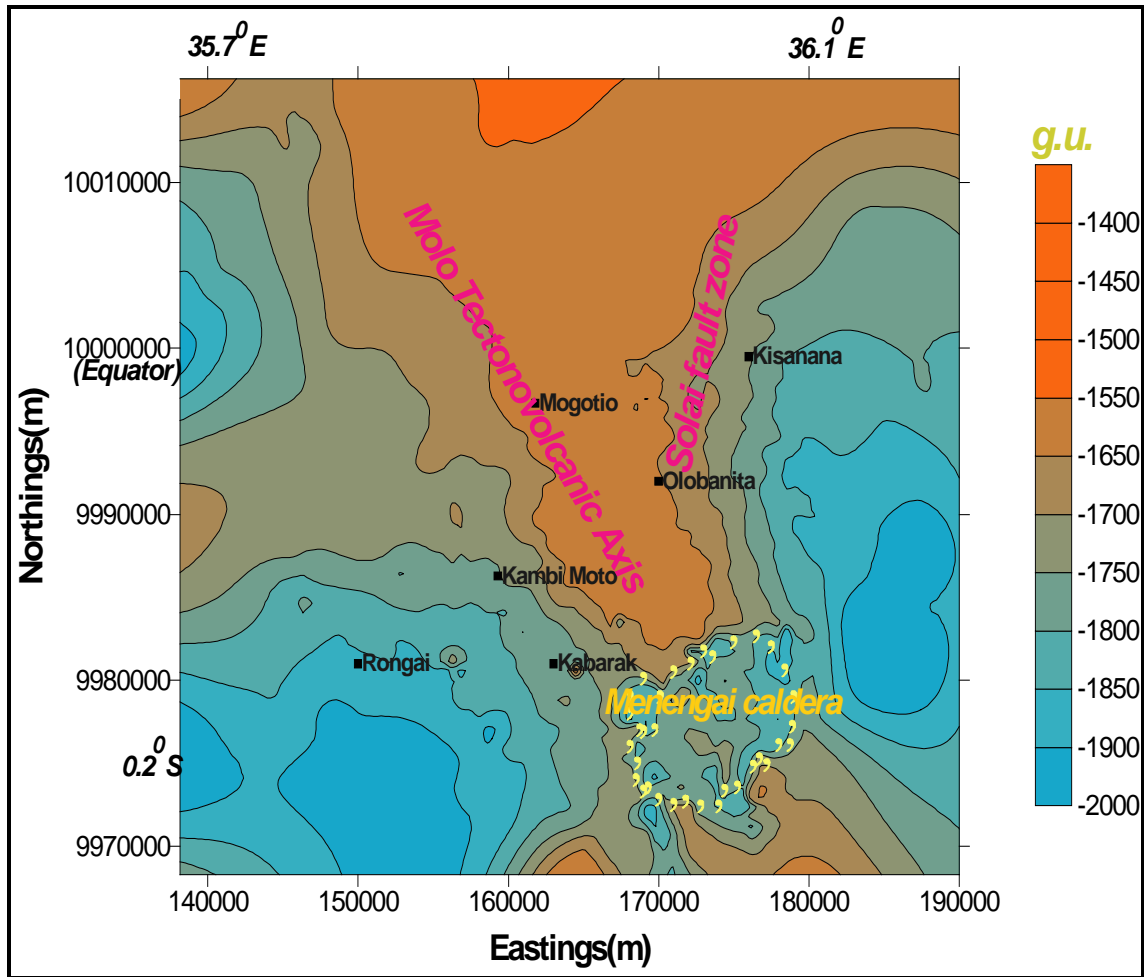
Figure 2.2: Gravity contour map of Menengai using Bouguer density of 2.8 gcm^{-3} (KenGen, 2008).
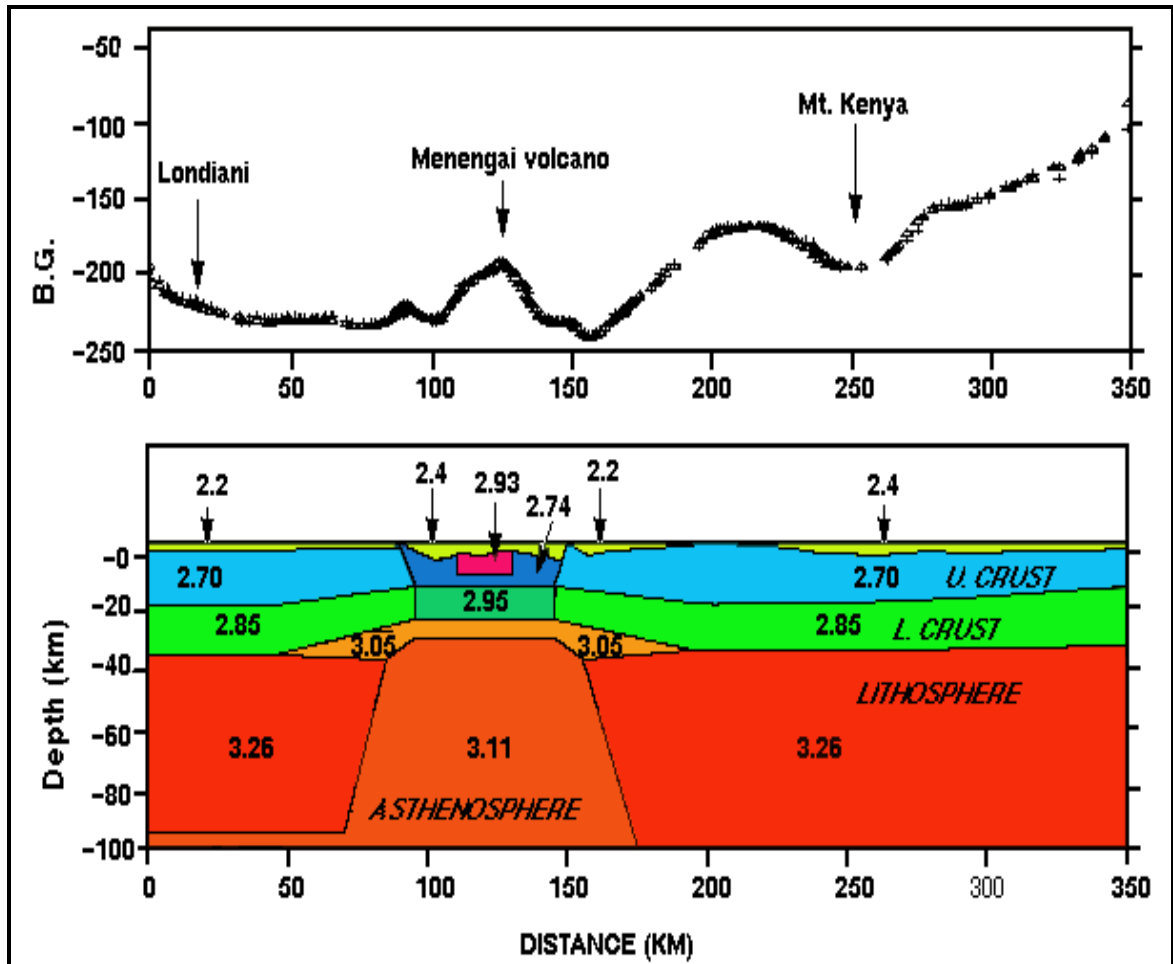
Figure 2.3: E-W gravity model across Menengai Volcano (modified from Simiyu, 1996). The top figure shows observed (plus) and predicted (triangle) Bouguer gravity. The bottom figure shows a density model with densities in g/cm^3 (Simiyu and Keller, 2001)
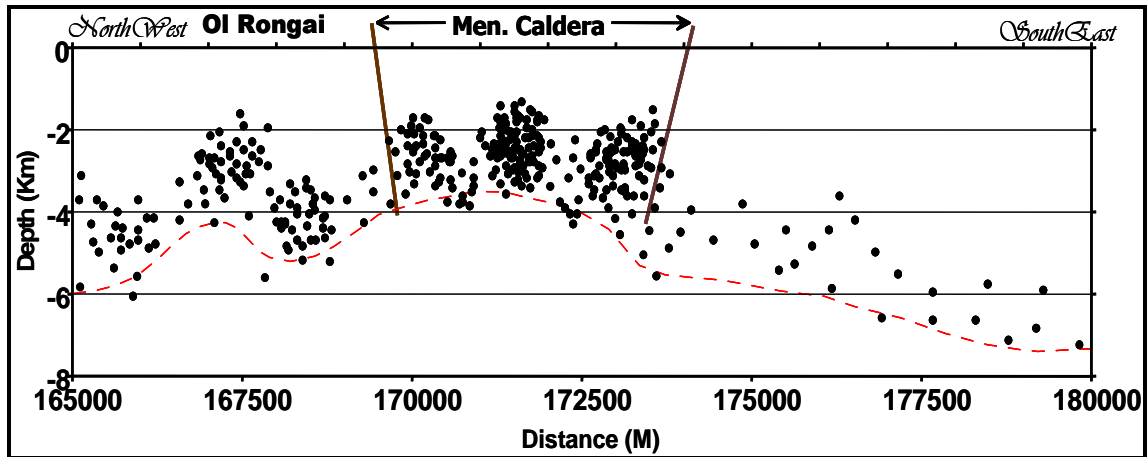
Figure 2.4: Depth distribution of micro-seismic events across Menengai volcano (modified from Simiyu and Keller, 1997).

2.1 THEORETICAL BACKGROUND

This section details the theoretical background of the methodologies used.

2.1.1 Magnetotellurics Method

The A/MT method is an electromagnetic (EM) sounding technique that uses surface measurements of the natural electric (E) and magnetic (B) fields to infer the subsurface electrical resistivity distribution. This method relies on the detection of small potential differences generated by electromagnetic waves propagated from the ionosphere (Ward and Wannamaker, 1983).

The natural source of MT fields originates from lightning discharges and magnetospheric current systems set up by solar activity. These sources create a spectrum of EM fields in the frequency band 10^{-4} to 10^{4} Hz that provide information used to

19

delineate structures at depth, from a few tens of meters to the upper mantle (a few tens of kilometers).

MT data at various frequencies provide a means to distinguish spatial variations in resistivity vertically and laterally. The EM field penetration, which decays exponentially, is related to the frequency and resistivity of the medium. Higher frequencies map the near-surface resistivity distribution. Lower frequencies that penetrate deeper provide information on deeper structures.

In this method, the magnetotelluric field is measured by its inductive effect on a coil or by use of a fluxgate magnetometer.

The apparent resistivity is calculated from the ratio of E and B magnitudes using the Cagniard equation of 1953.

$$\rho_a = \frac{0.2}{f} \left| \frac{E}{B} \right|^2 \quad \text{...................(i)}$$

where:

ρ_a = apparent resistivity (Ωm)

f   = frequency (Hz)

E   = electric field (mV/km)

B   = magnetic field (gammas)

The skin depth, Z, to which the MT field penetrates as a function of frequency and resistivity is given by the Kaufman & Keller equation developed in 1983 as:

$$Z = \left(\frac{2}{\omega\mu\sigma}\right)^{1/2} \quad \dots\dots\dots\dots\dots \text{(ii)}$$

$$= K\sqrt{\left(\frac{\rho}{f}\right)} \quad \dots\dots\dots\dots\dots \text{(iii)}$$

Where: K = 503 (constant);

Z = skin depth (m);

ρ = resistivity of the substrate (Ωm);

f = Frequency associated with MT field (Hz);

ω = angular frequency;

μ = magnetic permeability (H/m);

σ = conductivity (s/m).

The apparent resistivity for decreasing frequencies thus provides resistivity information at progressively increasing depths and is essentially a form of vertical electrical sounding.

Near surface resistivity inhomogenities have been found to distort the electric field since the field is discontinuous across a resistivity boundary. This distortion is known as static shift. This effect shifts the MT sounding curve (of apparent resistivity versus period) by some constant scale factor. Since the magnetic field is relatively unaffected by static shift, a controlled source magnetic field sounding such as TEM can be used to correct for static shift. The MT sounding curve is shifted vertically so that the high frequency part of the MT curve coincides with the TEM curve. The low frequency MT curve then gives an undistorted view of the deep resistivity section (Jones, 1988).

2.1.2 Tipper and Induction Arrows

Both induction vectors and tipper data are MT parameters useful in subsurface body localization and mapping (Fox, 2003). The interpretation of tipper and real induction vectors has its basis in the coordinates of tipper extremes, which are caused by the presence of anomalous bodies (Ingerov, et al. 2009).

The geomagnetic transfer function between the vertical and horizontal magnetic field components can be expressed as real and imaginary induction vectors. The inclusion of the imaginary induction arrows in the examination gives a quantitative measure of the influence of a three-dimensional conductivity distribution in the investigation area (Marcus, 1999).

In the Wise-Schumucker convention (Schumucker, 1970; Rokityansky, 1982), the real induction arrows point towards a more resistive region, perpendicular to the strike of

the lateral resistivity contrast. Furthermore, in the period range of induction, we expect the imaginary arrows to be opposed to the direction of the real arrows. At the period of maximum induction, indicated by the maximum amplitude of the real induction arrows, the imaginary arrows change direction (Marcus, 1999).Simpson and Bahr (1956) have argued that the length of induction arrows is proportional to the intensity of anomalous current concentrations.

2.1.3 Impedance Ellipticity

Ellipticity is calculated using the definition given by Ranganayaki (1984):

$$\text{Ellipticity} = \left| \frac{Z'XX - Z'YY}{Z'XY + Z'YX} \right| \quad \dots\dots\dots\dots\dots\dots (iv)$$

(where the symbol Z' denotes rotated impedance tensor, X and Y represent orthogonal directions in a coordinate system)

Ranganayaki (1984) points out that this quantity is limited as a dimensionality indicator because even at places where $Z'XX = Z'YY$, the fields could be influenced by an anomaly and require a 3D resistivity structure in order to describe their variation. This has been shown to be true especially at low frequencies. This deficiency can be offset by calculating skew, which increases at low frequencies where the impedance tensor is affected by a larger volume of the earth.

Impedance ellipticity is useful in determining the response, and hence the structural dimensionality at a site. It can generally be assumed that the vertical component of the magnetic field, H_z, is near zero except where lateral conductivity changes and results in a vertical (H_z) component.

2.1.4 Transient Electromagnetic Method

In the central loop transient electromagnetic method (TEM), a steady current is transmitted in a transmitter wire loop laid on the ground at the area to be studied. This current is allowed to flow for a sufficiently long time to allow turn-on transients in the ground to dissipate as shown in figure 2.5. This steady current is then abruptly terminated in a controlled manner. At the instant of transmitter turn-off, eddy currents reproduce the static magnetic field in the transmitter loop but then decay rapidly. The decaying primary magnetic field induces eddy currents immediately below the transmitter loop. As the initial near-surface eddy currents decay, its distribution in the ground in turn induces a secondary magnetic field that also decays with time. This process continues over time with ever weakening secondary magnetic field inducing currents at increasing depth.

The magnitude and rate of decay of the secondary magnetic field is monitored by measuring the voltage induced in a receiver coil, placed at the centre of the transmitter loop, as a function of time after the transmitter current is turned off. This is then interpreted in terms of subsurface resistivity structure (A'rnason, 1989).
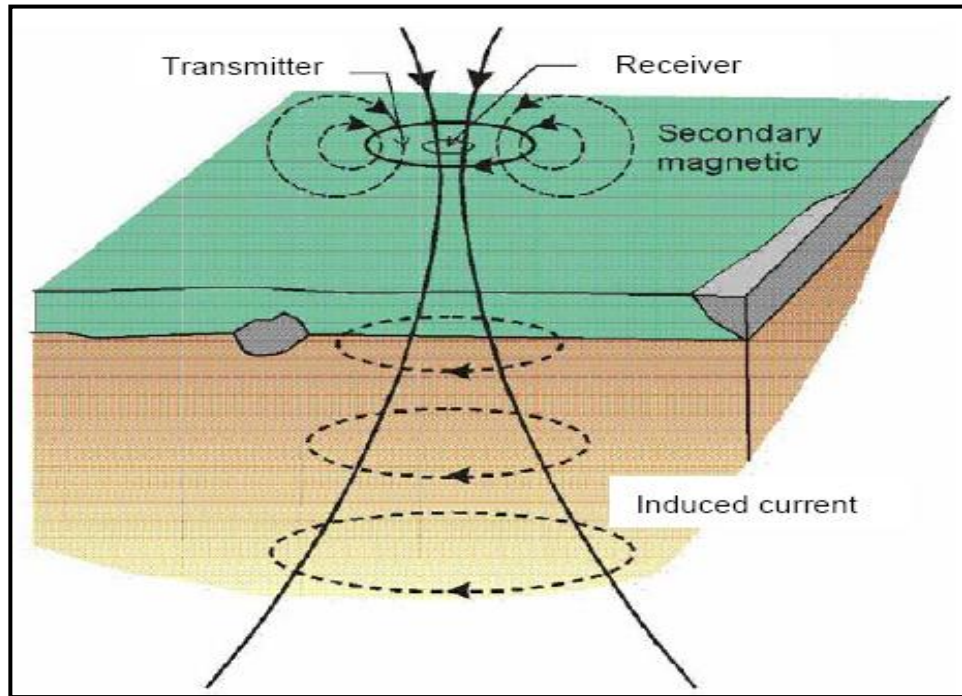
Figure 2.5: Transient current flow in the ground

Transient voltage generated in the receiver coil is given by (A'rnason 1989)

$$V(t) = \frac{I_o}{T_{off}} \int_{-T_{off}}^{0} V\_(t - \tau)\, d\tau \ \text{.....................} \ \text{(v)}$$

$$= \frac{I_o}{T_{off}} \int_{t}^{0+T_{off}} V\_(\tau)\, d\tau \qquad \text{.....................} \ \text{(vi)}$$

where T_{off} – time interval between successive current turn offs.

For homogeneous media of conductivity σ, the induced voltage in the receiving coil is approximated by A'rnason 1989

$$V(t,r) = I_o \frac{C(\mu_o \sigma r^2)^{2/3}}{10\pi^{1/2}t^{5/2}}$$

.... (vii)

where:

$$C = A_r n_r A_s n_s \frac{\mu_o}{2\pi r^3}$$

.... (viii)

The apparent resistivity ρ_a, in terms of induced voltage at late times after the source current is turned off is given by (A'rnnason 1989):

$$\rho_a = \frac{\mu_0}{4\pi} \left[\frac{2\mu_0 A_r n_r A_s n_s I_0}{5t^{5/2}V(t,r)} \right]^{2/3}$$

.... (ix)

where:

t   = time elapsed after the transmitter current is turned off;

A_r = cross-sectional area of the receiver coil (m^2);

n_r = number of windings in the receiver coil;

μ_o = magnetic permeability in vacuum (H/m);

A_s = cross-sectional area of the transmitter loop (m^2);

n_s =number of windings in the transmitter loop;

I_o = transmitter current (A);

V (t,r)   = measured voltage (V).

26

2.1.5 Geothermal Resource Estimation

The estimation of electrical power for a developed geothermal field may be done by either taking a rule of thumb working from the world average (Bertani, 2005) or by the lamped parameter model (Ofwona,2008) in which historical productivity is matched with physical observation and is used to predict productivity of fields under similar conditions.

In the case of undeveloped fields where there are either limited or no data necessary for numerical estimation of their geothermal electrical power potential, a generally accepted method for this estimation involves taking an average power generating capacity of a known geothermal field with similar geological conditions and using it to estimate the potential of an identified prospect area.

Experience from the nearby Olkaria geothermal field has shown that an average of 15MWe is generated using steam collected in one square kilometer of a steam field. The world average production ranges between 1.4 and 13.4 MW per square kilometer and is shown in Figure 2.6. For purposes of estimating the geothermal potential of Menengai, the Olkaria average was used.
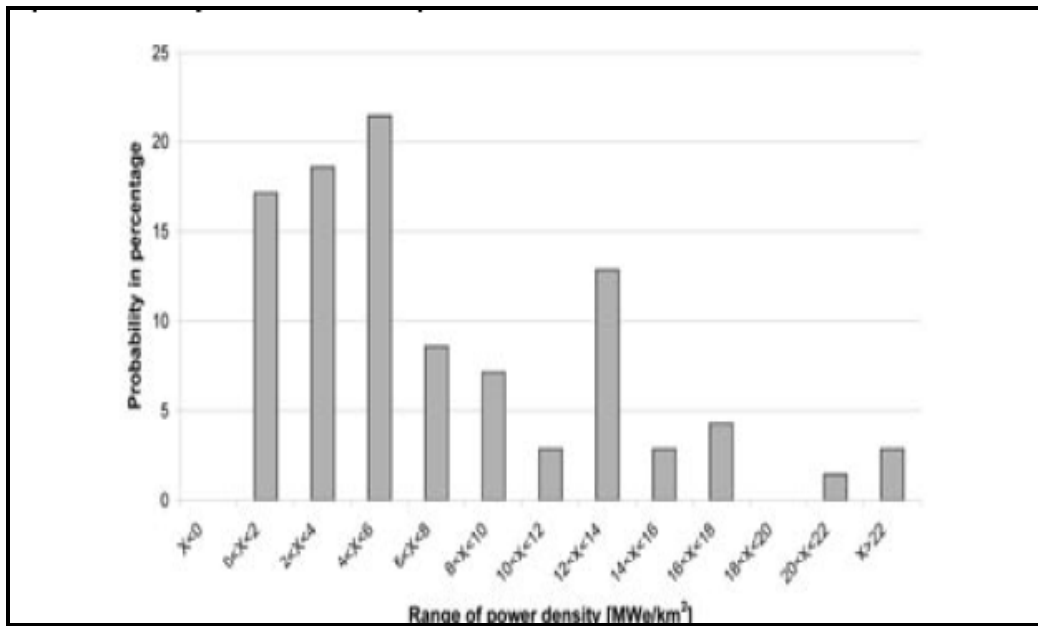
Figure 2.6: Power generation density distribution for 70 reservoirs across the world.

Modified from Bertani, 2005.

CHAPTER THREE

3.0 METHODOLOGY

This chapter deals with the field procedures, data collecting methods and their processing used in the study**.**

3.1 Transient Electromagnetic Method

In the transient electromagnetic (TEM) method an electrical current is injected into the ground and its decay and the magnetic field created are measured in order to infer the resistance of subsurface formations. The TEM method can effectively resolve earth resistivity structure down to 2 km.

For TEM soundings the Zonge system comprising the following equipment was used;

- AC Generator (415V)

- Transmitter- GGT-3

- Transmitter Controller-XMT-16

- Data logger- Geophysical Data Processor (GDP-16)

- Receiver coil- TEM/3

- Voltage regulator- VR-1

- GPS

A half-duty square wave current was transmitted into a 300m x 300m transmitter wire loop (Figure 3.1) at frequencies of 16 Hz and 4 Hz. The transmitter was synchronized with the data processor (GDP-16) so that at current turn offs the processor coil retrieved data from the receiver coil.
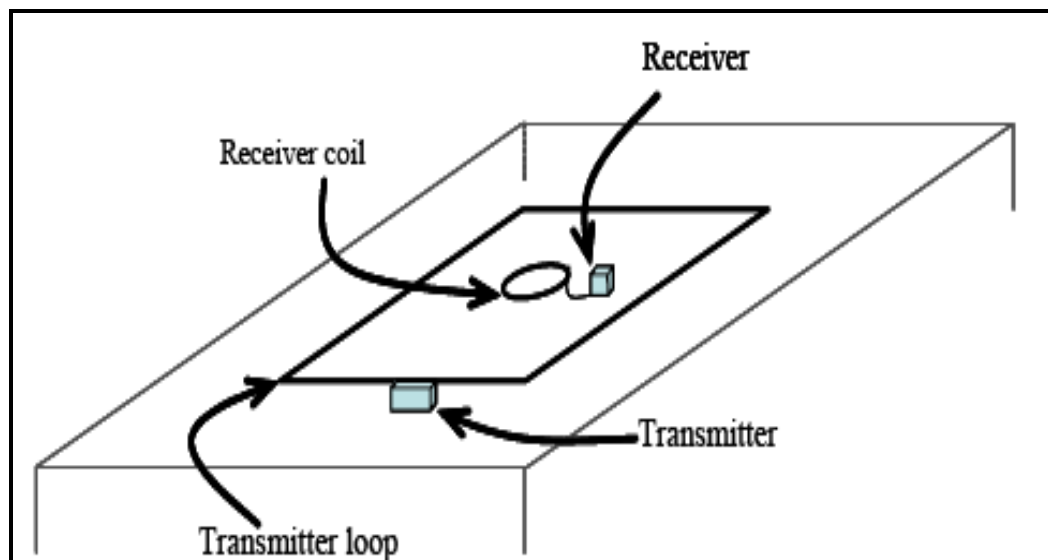
Figure 3.1 Central-loop time domain TEM field layout

3.2 Audio Magnetotelluric and Magnetotellurics Methods

In the magnetotelluric technique (MT) the fluctuations of the earth's natural electrical and magnetic currents are measured. Audio magnetotellurics (AMT) and MT methods are essentially the same, differing only in the frequency range captured. The lower the frequency, such as the case for MT, the deeper the penetration. The AMT technique acquires data in the frequency range of about 1 KHz to 10 KHz; which is roughly the range of human hearing and hence the 'audio' prefix.

The equipment used for an AMT/MT sounding were;

- An MT/AMT unit (MT-5A From Phoenix Geophysics, Canada).

- Electrical ports

- Electrodes

- Electric cables

- A car battery

- A compass

- GPS

To ensure good conductivity, the ports were soaked with clean water that had been salted with common salt. The three magnetic electrodes were buried at about 1 foot depth and oriented as shown in the directions shown in Figure 3.2. The four telluric ports were also shallowly buried with a solution of Bentonite. A car battery was used to power the system. The MT Unit collected data continuously for at least 18 hours at each station for MT and 1 hour for AMT.
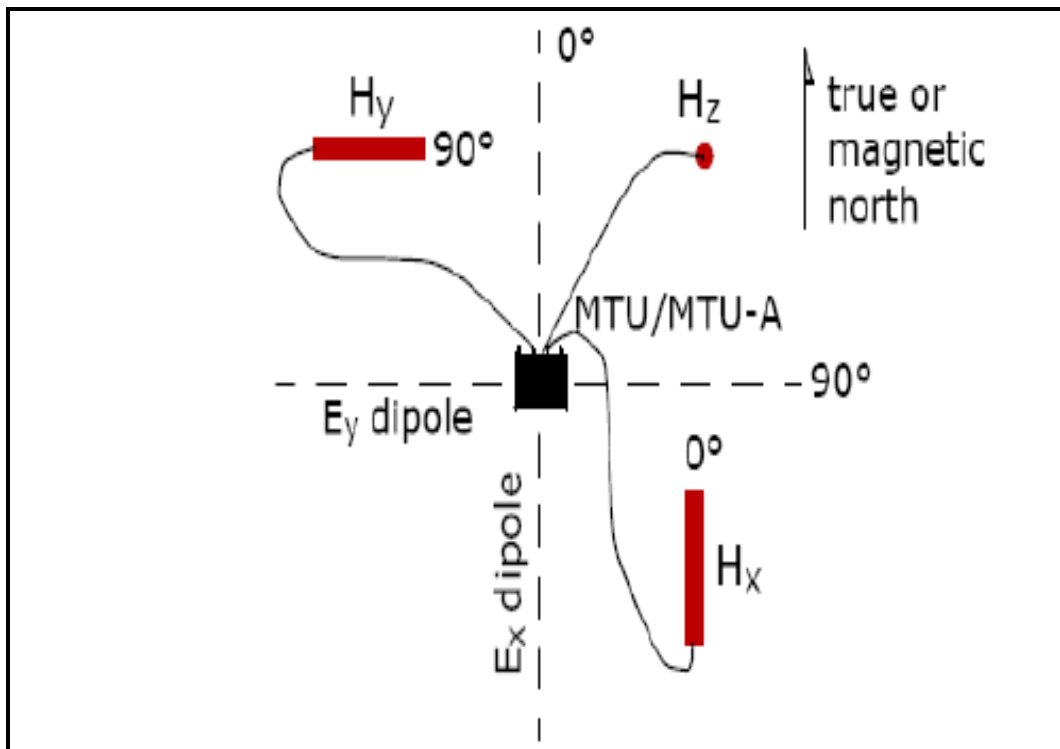
Figure 3.2 A field array for a 5 channel MT data acquisition system (from Phoenix Geophysics Ltd.)

In this study TEM soundings were carried out at the same stations with MT so that the static shift problem with MT could be resolved using TEM results. In a bid to obtain a clearer resolution of the near surface structure AMT soundings were also collected at the same stations as TEM and MT. These data were used to validate TEM data for shallow depths as well as provide a continuation of deep MT results to the shallow levels.

3.3 Data Analysis

Time-series data were downloaded using the SSMT2000 program from the MT unit and were processed using MTEditor provided by Phoenix Geophysics-Canada.The

SSMT2000 was used for configuring A/MT instrumentation and parameters. The MTEdit program accepts MT plots output by SSMT2000, merges the crosspowers and displays MT parameters graphically. It also enables elimination of crosspowers from the calculations and hence the possibility of editing out poor quality data.

The primary objective of editing is to create a smooth resistivity curve by eliminating those cross powers that have been moved too far from the mean by noise and related effects. Though it is possible to eliminate data points from being considered, the software does not delete them completely. It places a mask on those unwanted crosspowers, allowing one to revert to the original data at any time.

The resulting data were then converted into the electronic data interchange (EDI) standard industry format accepted by the WinGlink™ Intergrated Interpretation Software. A well established method for static shift correction of MT data is the use of TEM (Stenberg et al, 1988; Pullerin and Hohmann, 1990). The imported 1D model is used to calculate a forward MT response. The observed apparent resistivity curve can then be shifted along the resistivity axis to coincide with the values suggested by the TEM response.

Joint inversion of A/MT and TEM data is performed to deduce 1D smooth (Occam and Bostick) models of the subsurface resistivity structure as well as resistivity isomaps at different depths, elevations and periods/frequencies. Layered resistivity models are then calculated from the smooth models. Four profiles shown in figure 3.3 were taken to delineate the depth and geometry of observed resistivity results which are presented in the form of contoured models. Some of the 1-D models are shown in appendix II.

3.4 Estimating Geothermal Resource Potential

In estimating the potential electrical generating capacity of a prospect area, the total prospect area is determined using resistivity data. The area under the 20 Ohm-m contour roughly estimates the top of a geothermal reservoir (KenGen, 2004).

Assuming that the calculated anomalous area under the contour to be A, square kilometers and Q is the expected average electrical power generating capacity per unit area in Mega Watts of electricity per square kilometer then the estimated power generating potential for a geothermal area can be expressed as,

Power Potential = A (Km^2) x Q (MWe / Km^2) …………………. (x)
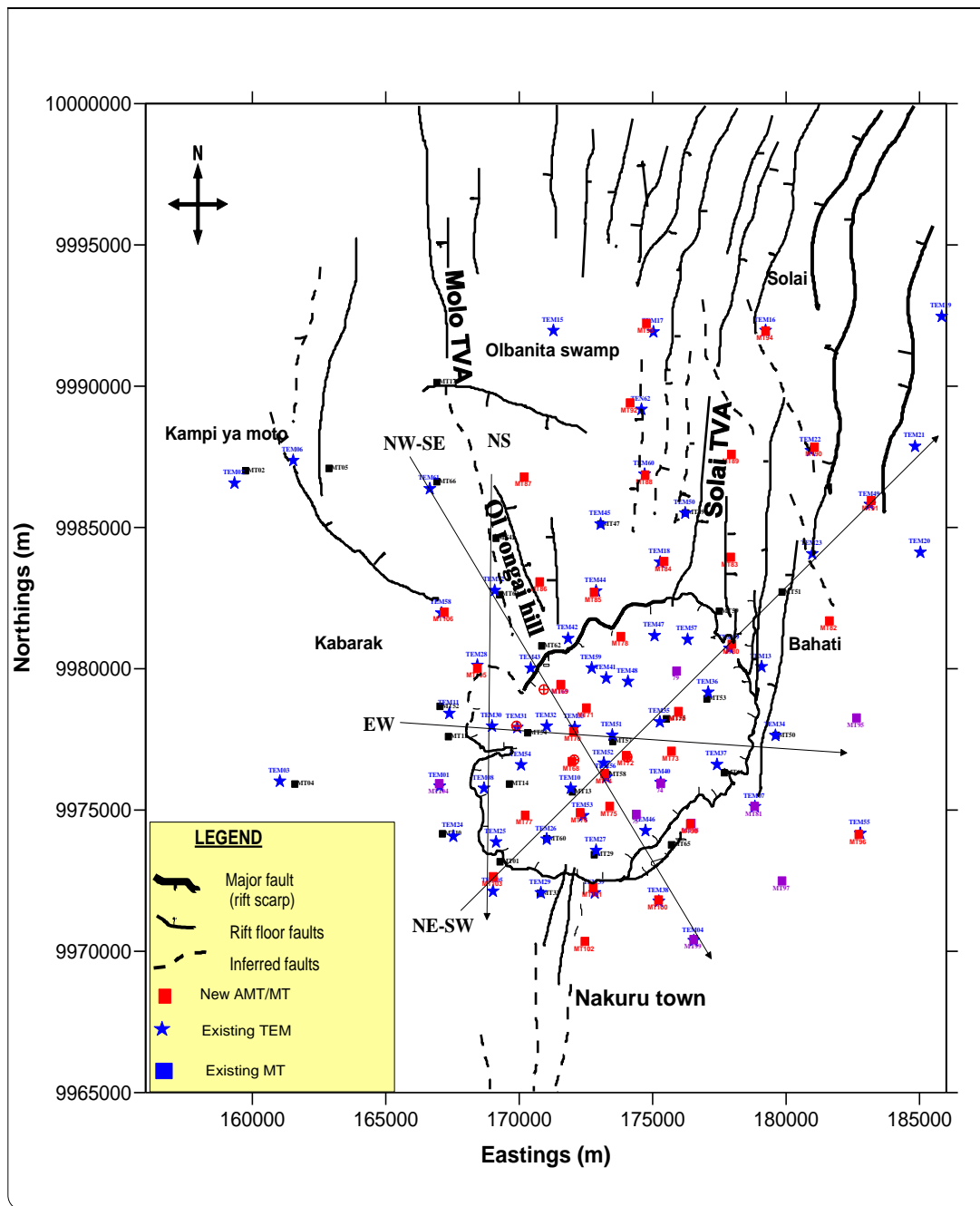
Figure 3.3 A map showing the stations at which MT, AMT and TEM data were collected at Menengai.

CHAPTER FOUR

4.0 RESULTS AND DISCUSSIONS

The following section presents the results and deductions arrived at after the data analysis procedures outlined in chapter 3 were applied. The main software used in the interpretation of these data is WinGlink software while data presentation was facilitated with Surfer and Corel Draw software

4.1 RESISTIVITY ISOMAPS

In this section, contoured resistivity distribution maps based on the Occam inversion were prepared using the WinGlink software. Maps were created and displayed as contour and color filled maps of different values associated with a given parameter at a project station. The values used to build up these maps are of two kinds; the values of the parameter at each data collection station and the interpolated values of the same parameter. Gridding parameters are specified so that suitable grid steps are taken based on the parameter values. For the maps shown in this section grid steps of 798.4 m were the software default values and were used with normal gridding option at 5m interpolation radius and zero smoothing factor.

These maps present results from the joint inversion of the TEM, MT and AMT data at various depths.

4.1.1 Resistivity Map at 1500 m.a.s.l

Most of the area at this level is relatively conductive with some resistive formations apparent in the SE sector of the caldera as shown in figure 4.1. A 10 ohm-m

resistivity formation emanating from the SW intrudes into the caldera from the western wall where the Molo TVA coincides with the caldera. Another low resistivity region occurs north of the caldera and spreads towards the north east connecting the two TVAs in the area.
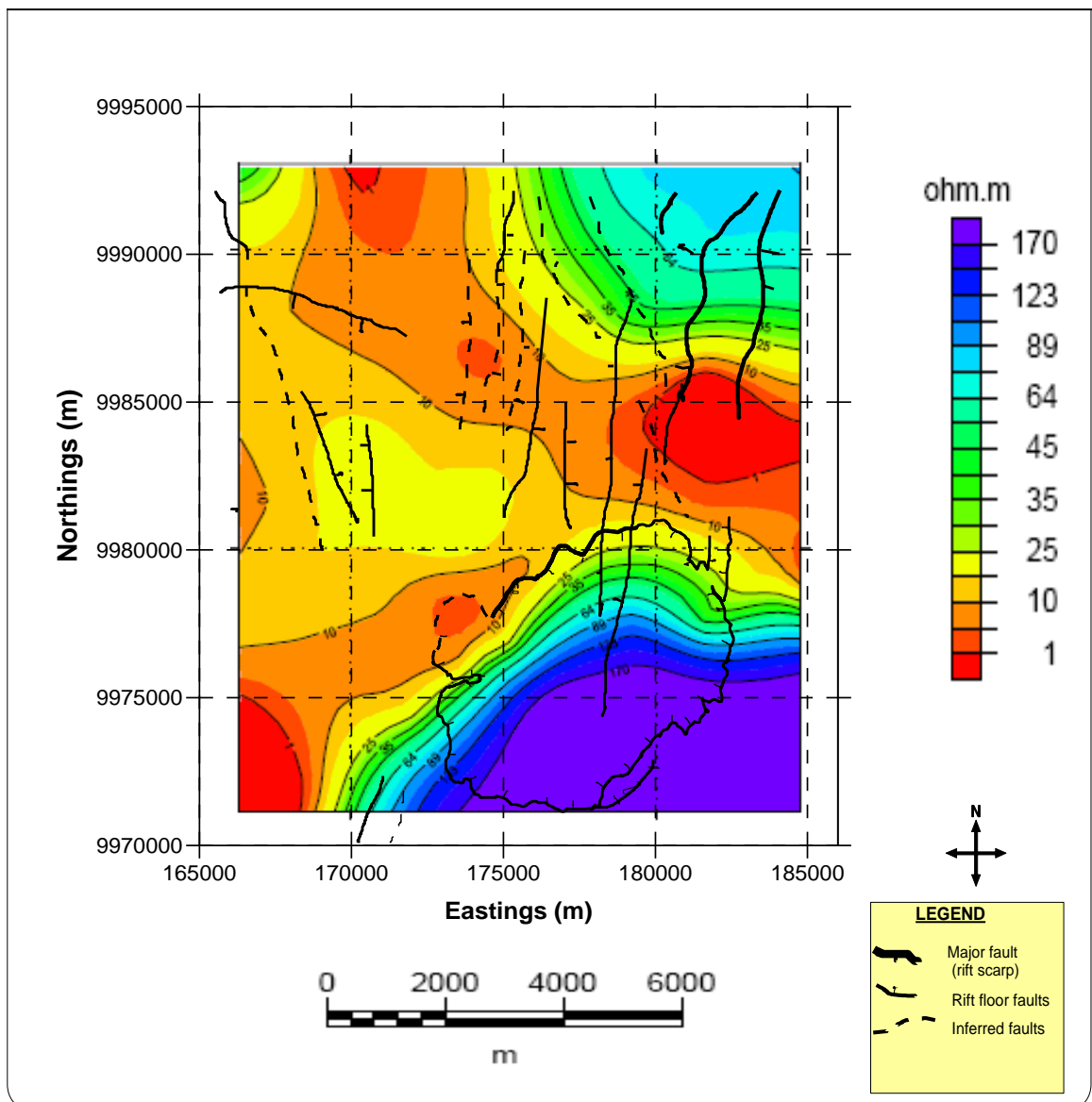
Figure 4.1: A resistivity map interpolated at 1500 masl elevation based on Occam inversion

4.1.2 Resistivity Map at 1000 m.a.s.l

At this depth, a major NE-SW trending structure separating high (to the south east) and low (to the south west and centered) resistivity signatures cuts across the study area as in figure 4.2. This structure coincides with the Solai TVA. The central low resistivity section may be controlled by the north south trending fault system.
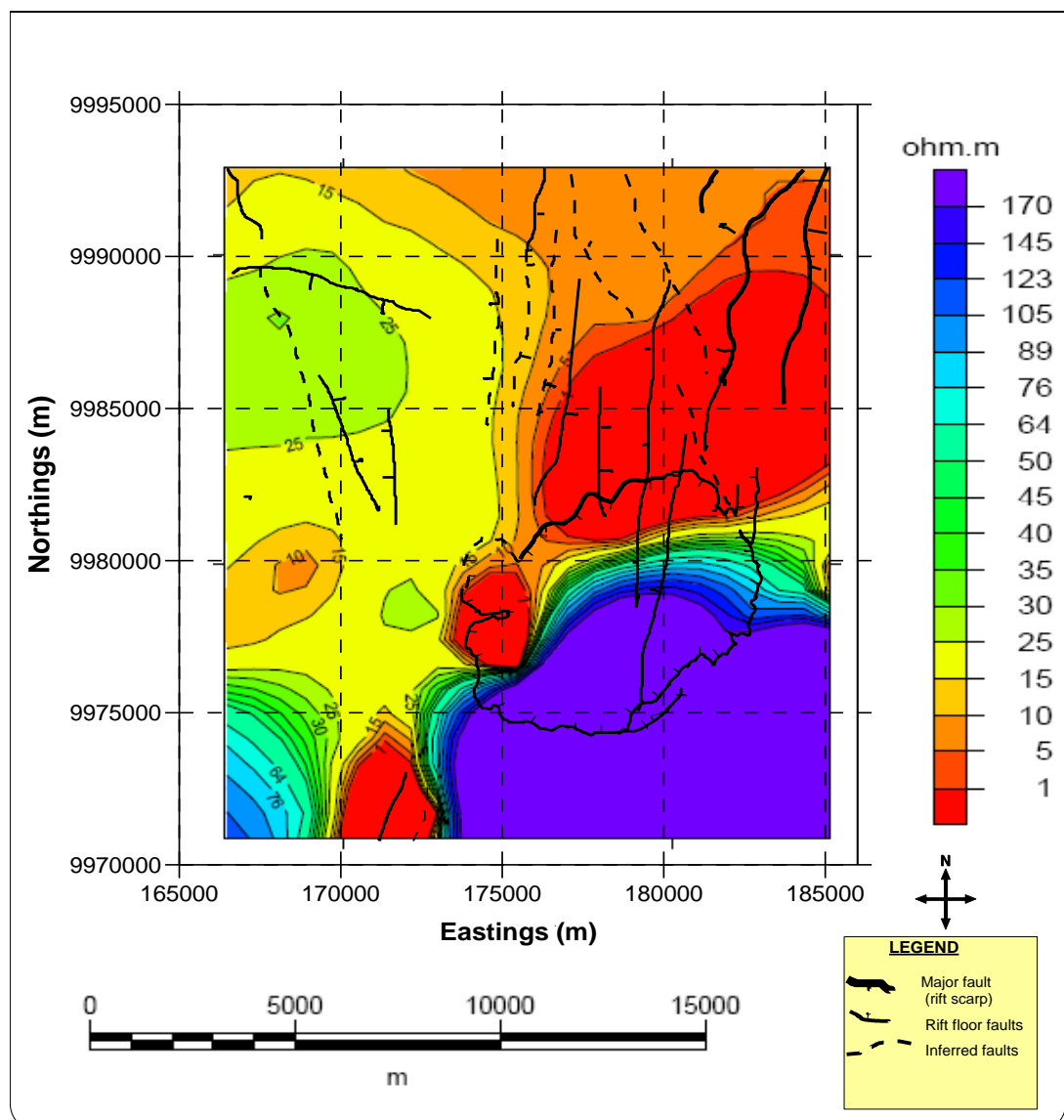
Figure 4.2: Resistivity map interpolated at 1000masl elevation based on Occam inversion

4.1.3 Resistivity Map at Sea level

A low resistivity region (less than 35 ohm-m) trending NE-SW separates two regimes of resistive formations and coincides with the NW caldera wall as demonstrated in figure 4.3. A conductive zone of about 20 km^2 caused by hydrothermal alteration is inferred.
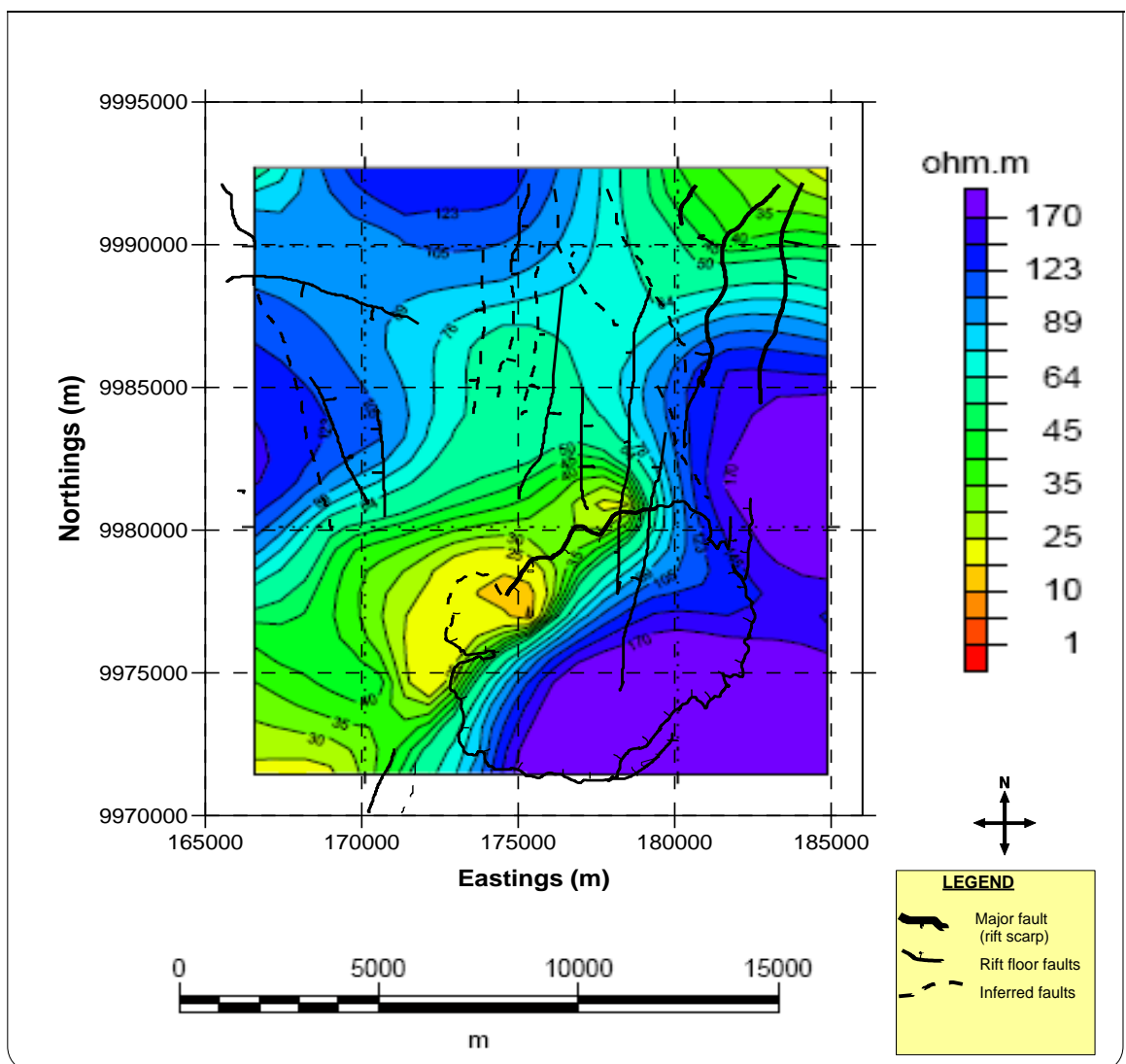
Figure 4.3: Resistivity map interpolated at 0 masl elevation based on Occam inversion

4.1.4 Resitivity Map at 1000 m.b.s.l

Figure 4.4 shows a North-South trending low of ~40 ohm-m is surrounded by resistive structures of ~120 ohm-m to the east and west. The low trending NE-SW is still apparent. Much lower (~5 ohm-m) signatures are observed along the southern caldera wall.
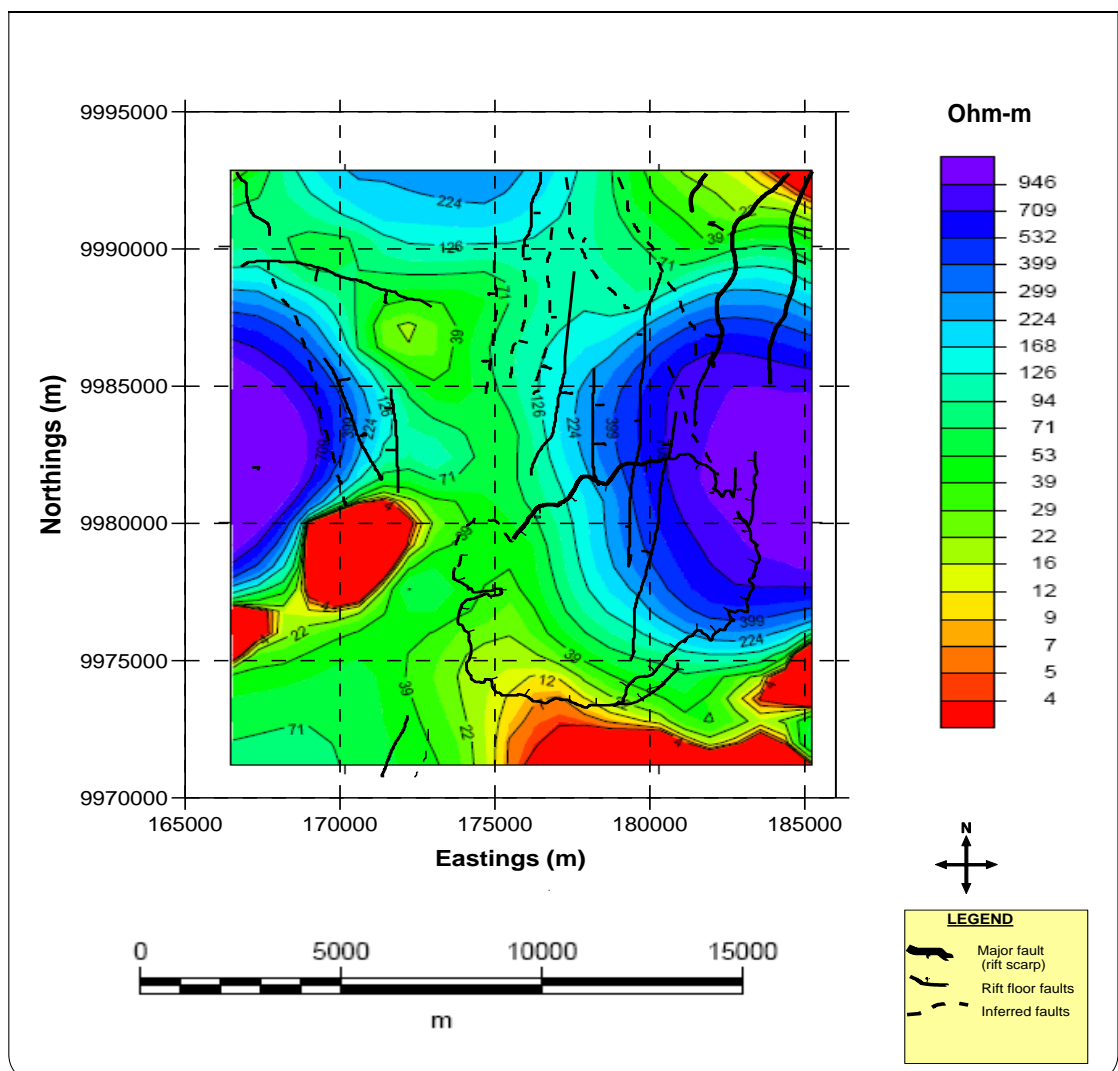
Figure 4.4: Resistivity map interpolated at -1000 masl elevation based on Occam inversion

40

4.1.5 Occam Resistivity Map at 3000 m.b.s.l

At 3000mbsl shown in figure 4.5, a low still persists to the west and a large high to the East. The north western part of the caldera remains very low (<5 ohm-m).
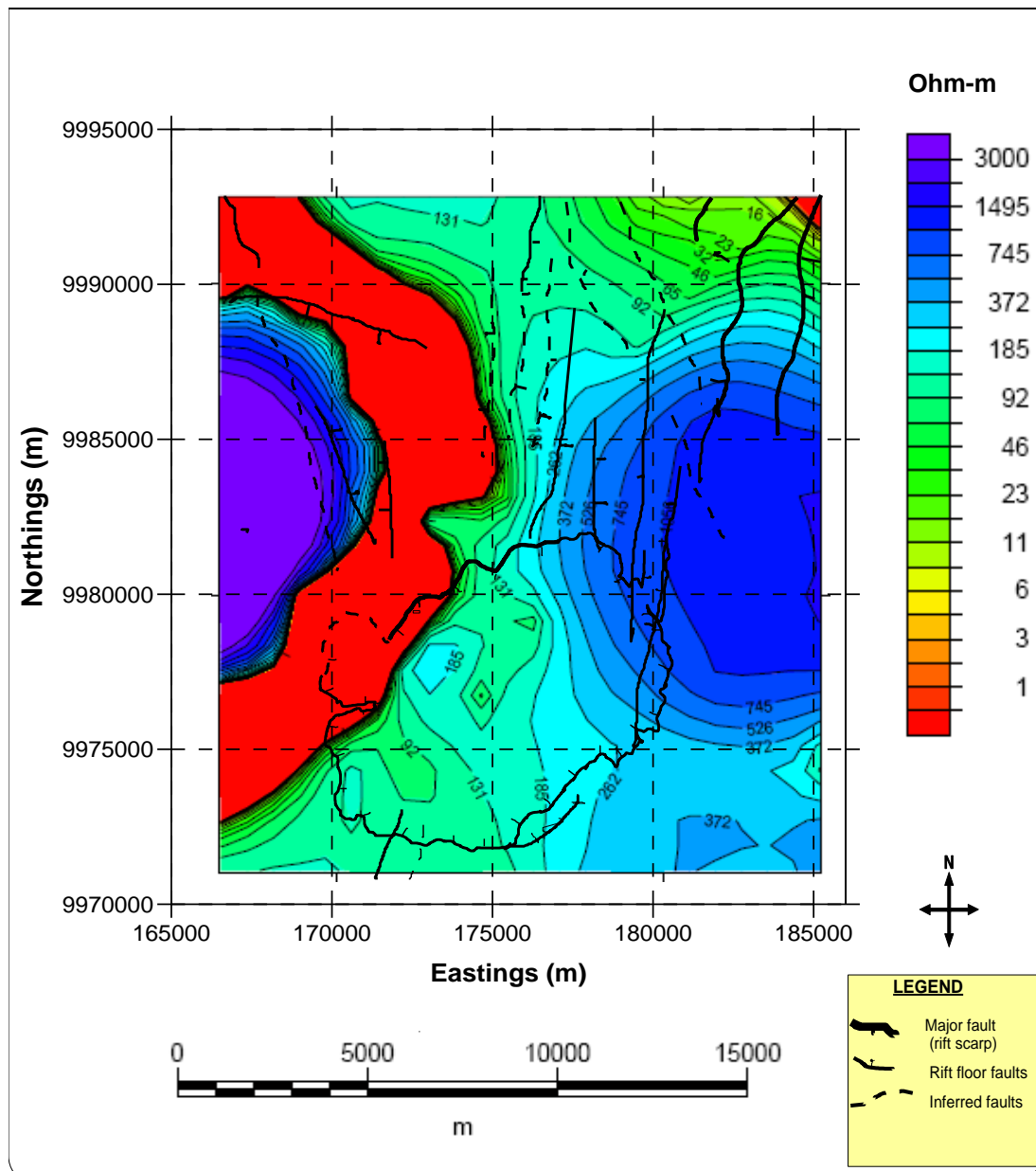
Figure 4.5: Resistivity Map interpolated at -3000 masl elevation based on Occam inversion

4.2 RESISTIVITY MODELS

To better examine the resistivity variations at depth, four cross sections (Figure 3.3) were taken across the geological structures in the area. These 2-D cross sections are shown in figures 4.6 to 4.9.

4.2.1 E-W Profile

The East-West profile shown in Figure 4.6 shows regions of high resistivity (>120 ohm-m) are observed on the ends of the profile. A low resistivity anomaly (<20 ohm-m) cuts across the central region at 500masl. A more conductive cap is observed across the region.

There are two possible reservoirs observed on the profile. The first of these occurs in the area below TEM 35 and TEM 37 (between 7000m and 11,000m from the origin of the profile). However, very few measurements were carried out in the eastern end of the caldera to conclusively study it. This anomalous region is separated from the second one by a deep conductive segment that originates from the eastern caldera wall. This conductive zone may be the area where meteoric waters mix with hot geothermal water. Ionized cooler water flows deeper and the buoyant hot water rises.

The second reservoir occurs to the west and intrudes the western caldera wall extending to the central caldera area. The resistive body (>120 ohm-m) extends from about sea level to depth with a shallow conductive cap at about 500m depth. We attribute the resistive body to the hot reservoir with a conductive cap of thermally altered material.

Figure 4.6: The East-West resistivity profile

43

4.2.2 N-S Profile

The North-South profile that cuts across the western sector of the caldera presented in figure 4.7 shows two high resistivity regimes. The first of these anomalies occurs directly below Olrongai Hill and is characterized by a resistive body at about 500masl that is enclosed by two conductive regimes. The trend of the outlined body aligns with the Molo TVA. This regime is separated from the second one by a narrow vertical feature with low resistivity that coincides with the northern caldera wall and runs deep.

In the second anomaly, a thick conductive segment, about 500m thick, separates surface resistive rocks with a successively increasing resistive section that runs deep reaching some 6000m depth from the surface. This anomaly shows classical geothermal reservoir characteristics. Meteoric recharge is interpreted to enter the system through the fractured caldera wall to the South and the waters are heated as they percolate through hot rock and mix with heated geothermal water. A similar scenario is observed at the northern boundary of the caldera.

Figure 4.7: The North-South resistivity cross

45
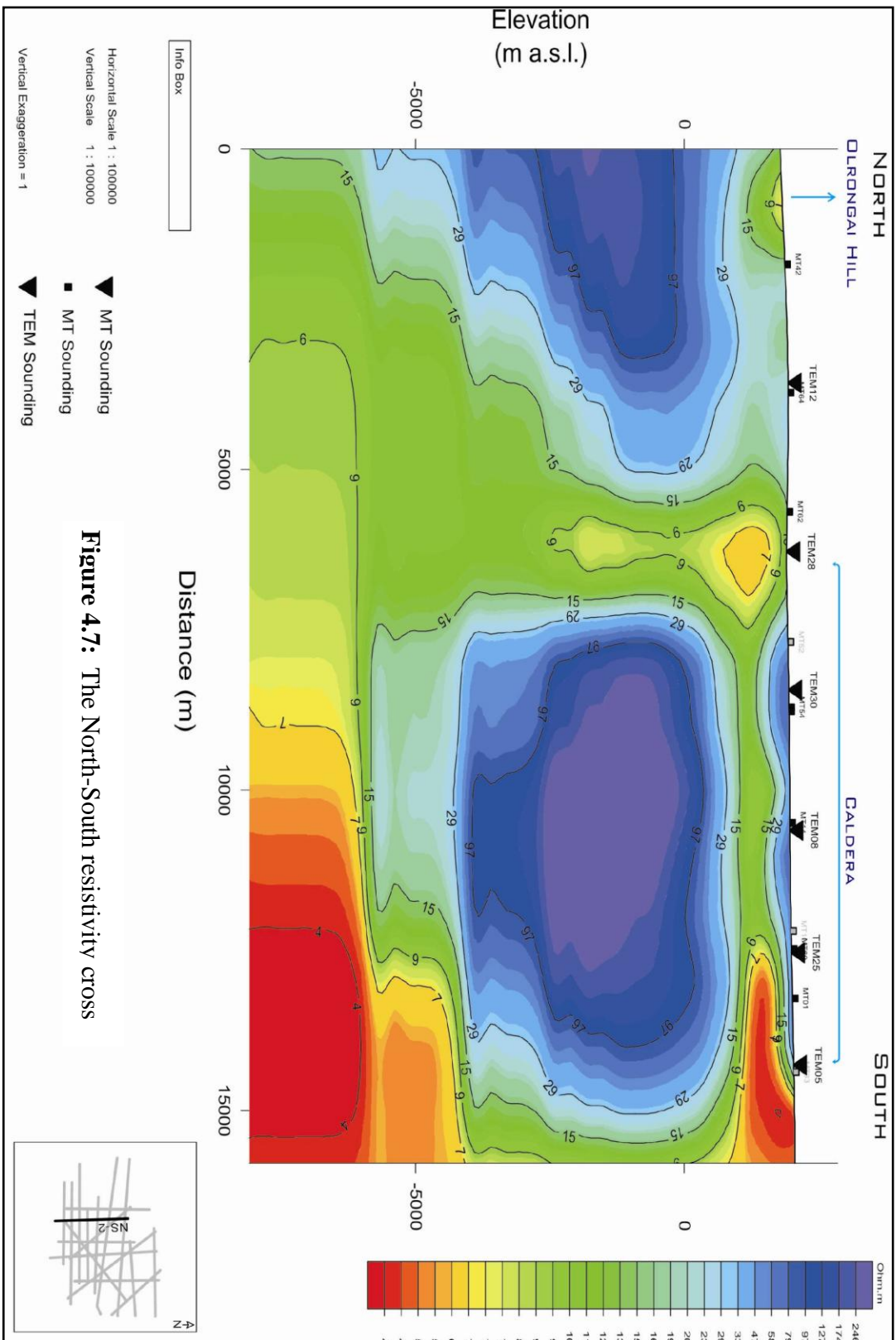
4.2.3 NE-SW Profile

In figure 4.8, a resistive intrusive coincides with the Solai TVA to the north east with formations extending upwards from about 500m depth to the surface. This structure delineates the extent of the interpreted geothermal system to be confined within the bounds of the caldera.

An anomaly located between 2000m and 9000m along the profile may be associated with a reservoir. It is observed to diminish both in size and resistivity signature to the Northeast. This profile shows that the system observed in the eastern part of the caldera may be viewed as being independent to that located at the centre of the caldera that extends both westwards and southwards.

4.2.4 NW-SE Profile

Two regions of high resistivity are observed on the profile shown in Figure 4.9. The first anomaly is positioned beneath Olrongai hill and occurs slightly deeper (500mbsl), rather than 500masl in the former, and extending to depths greater than 6000m.

More importantly, a significant resistive body is observed to the SE enveloped by a conductive cap. This anomaly is interpreted to represent a geothermal reservoir lying between TEM 33 and TEM 46 (Bottom width of 7.5km). The conductive cap is enclosed by a resistive sector and lies between sea level and approximately 500masl. The section is subsequently punctuated with progressively resistive formations characteristic of a typical geothermal reservoir.

Figure 4.8: The North East- South West resistivity cross section

Figure 4.9: The North West-South East resistivity cross section
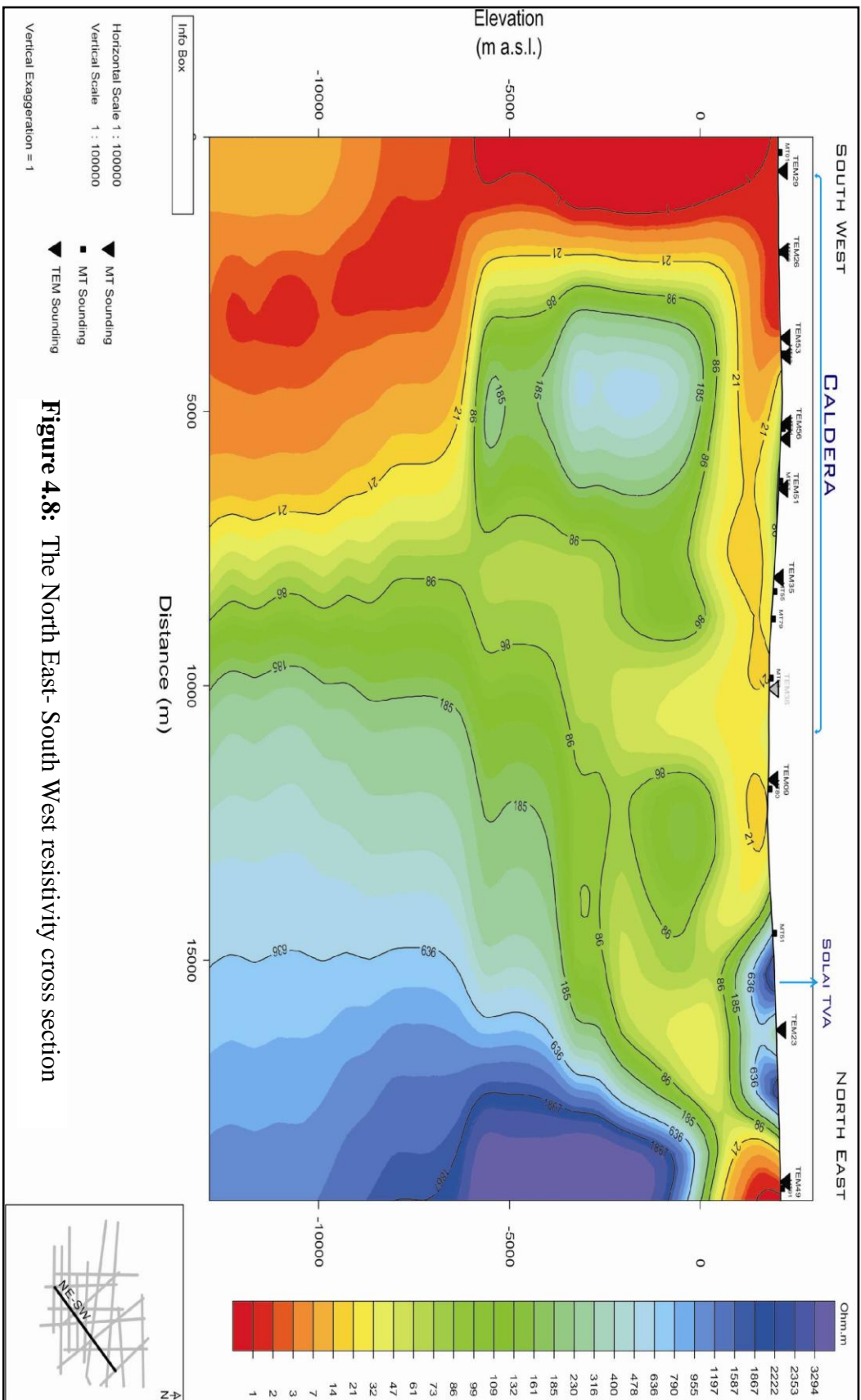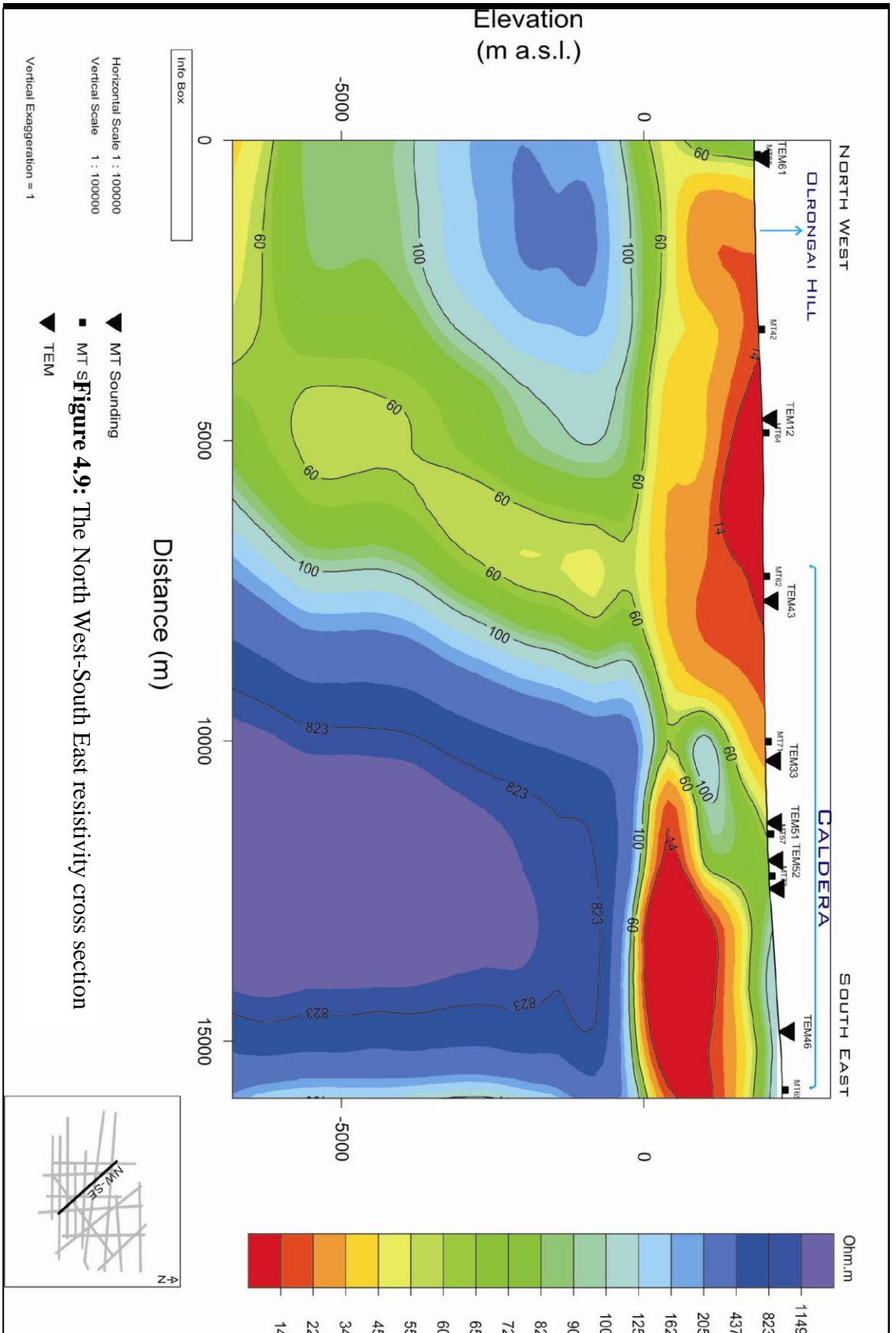
4.3 Tipper Data Results

Tipper data from the Menengai area presented in figure 4.10 (a) and (b) show extremes of phase and magnitude at two distinct locations. One anomaly trends in a SW-NE fashion and meets the caldera wall to the West. This anomaly has already been delineated with resistivity as shown in see figure 4.3. The second anomaly coincides with the N-S trending resistivity anomaly that meets the caldera walls to the as shown in figure 4.4. There is also a central anomaly shown in figure 4.10 (b) that has also been mapped with resistivity in figure 4.2.

This confirms the presence of localized bodies beneath Menengai causative of the anomalies in the western sector, central sector and the southern sector of the caldera.
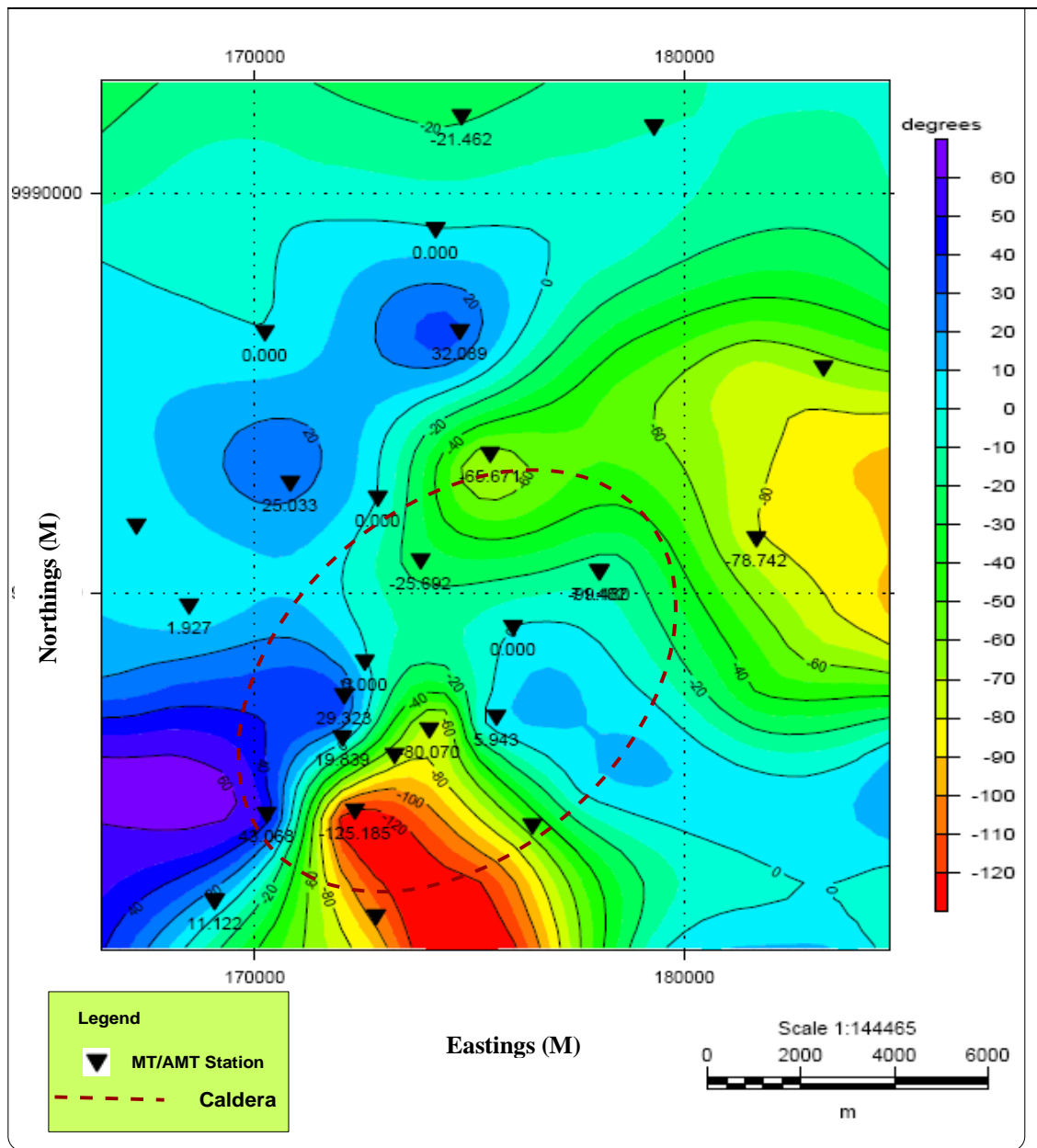
Figure 4.10 (a): Tipper Phase taken at a period of 10s
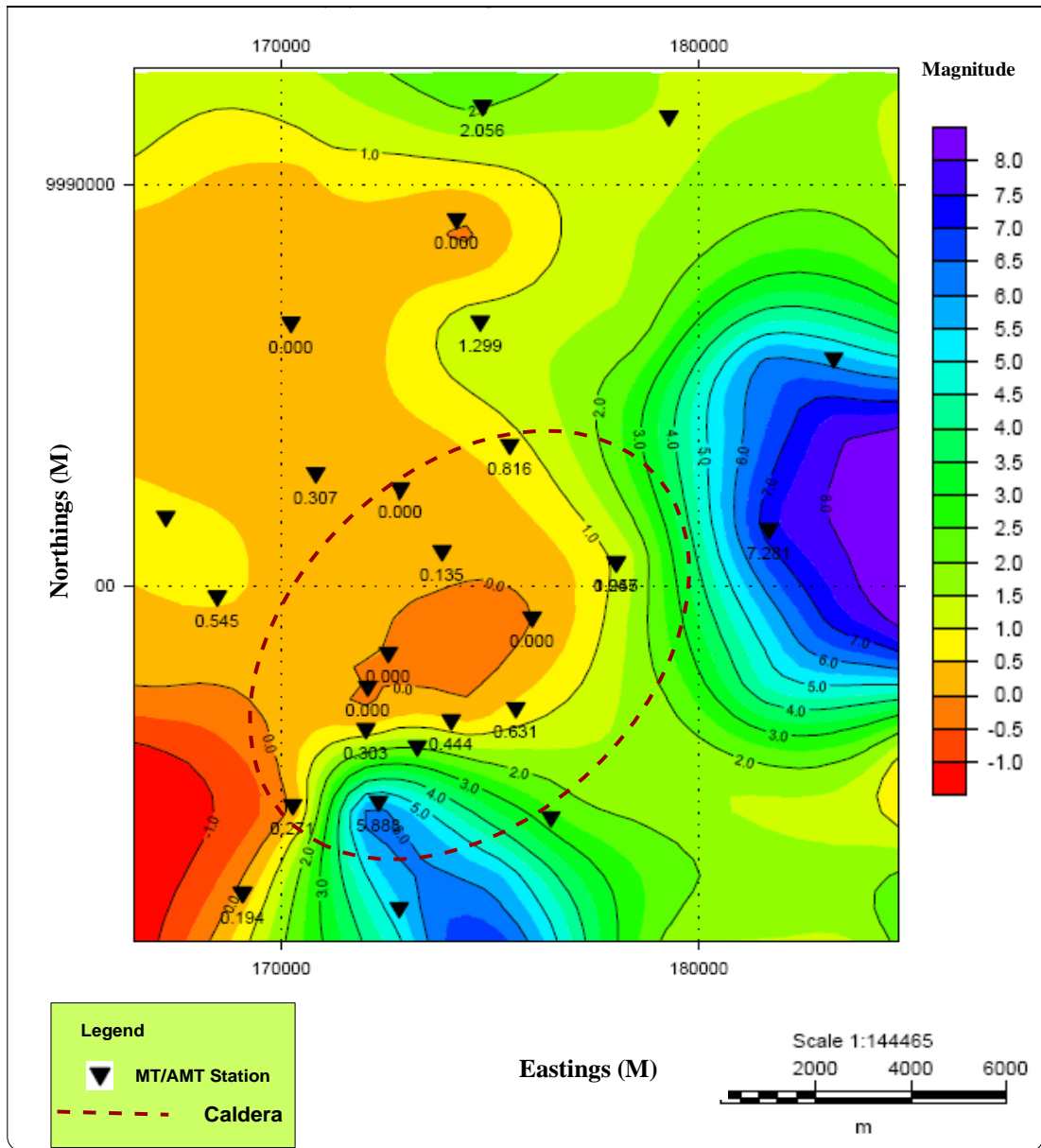
Figure 4.10 (b): Tipper magnitude taken at a period of 10s

4.4 Induction Arrows

Figure 4.11 shows the real induction angles taken at Menengai at a period of 10 seconds. The arrows show three conductive centres. The first of these centres is located in the central part of the caldera and extends towards the north eastern

boundary of the caldera wall. The second is located at the western caldera wall and the third intrudes the caldera from the southern boundary.
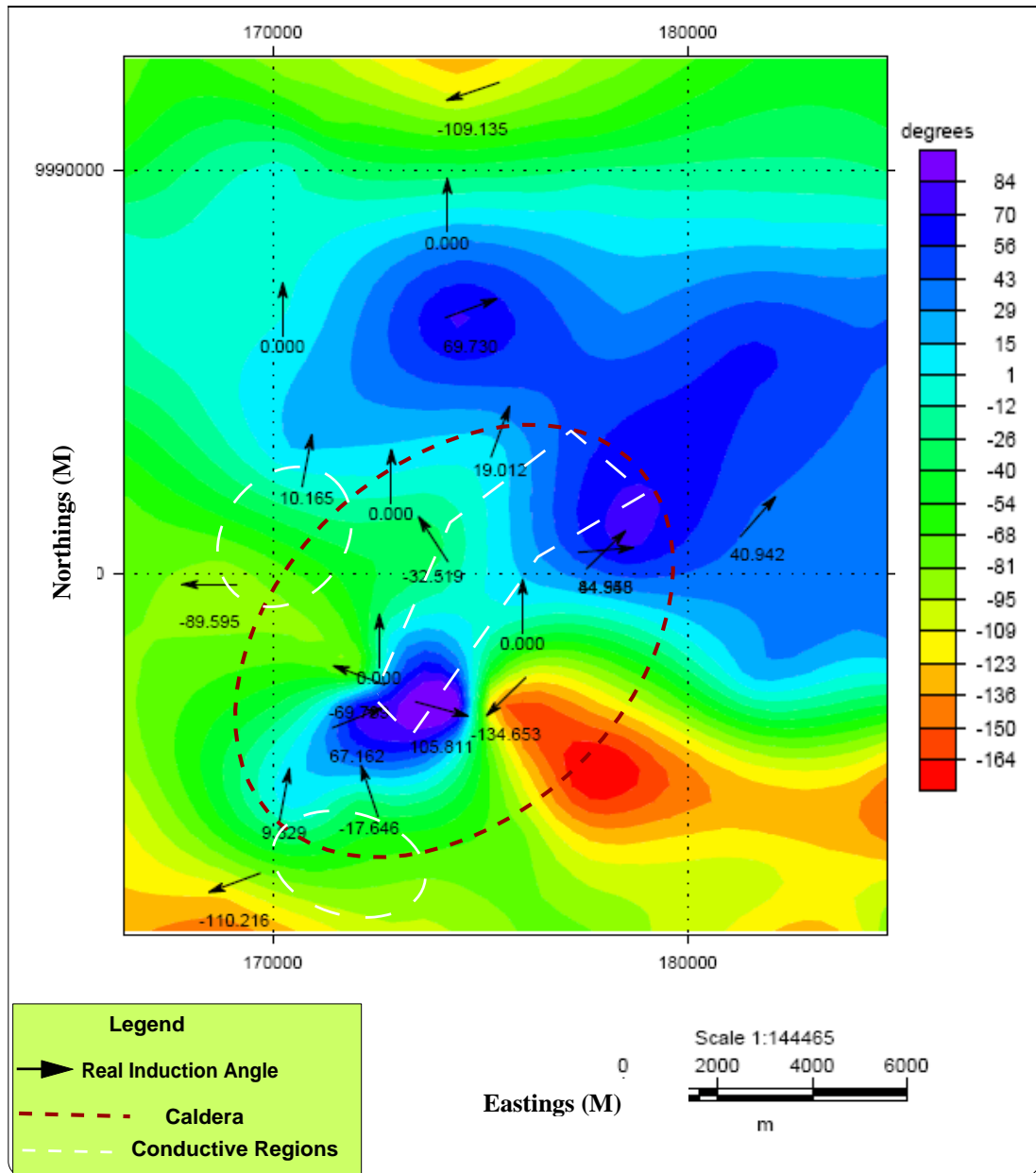
Figure 4.11: The real induction vectors at a period of 10s.

In figure 4.12, both real and imaginary induction arrows are shown for three different frequencies. For the higher frequencies as in figures 4.12 (a) and (b) the length of the

arrows is somewhat uniform implying that current distribution is near homogeneous. The highest current anomaly in figure 4.12 (c) is observed at the lowest frequencies corresponding to late time implying deeper resistivity in-homogeneities.
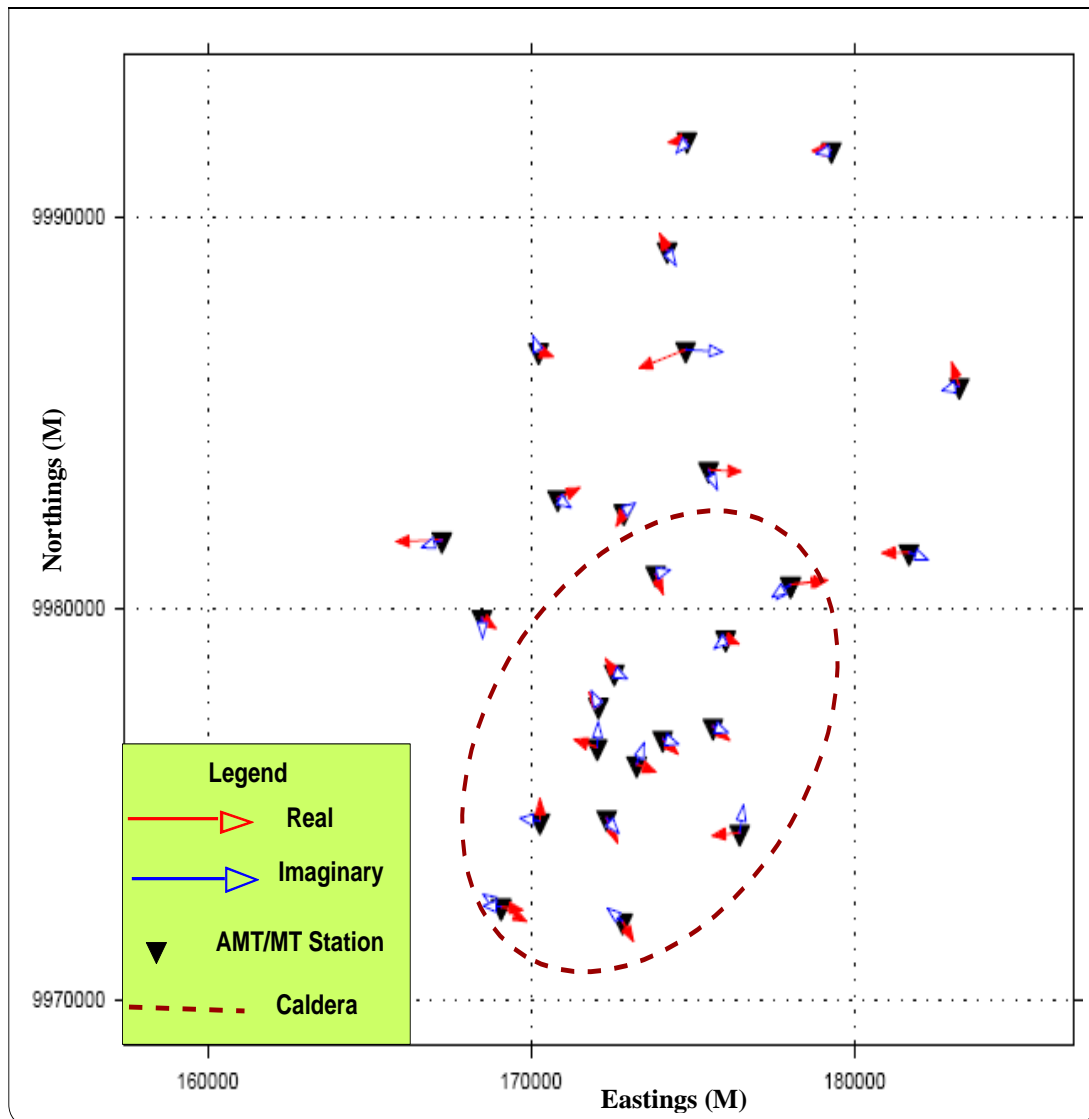
Figure 4.12 (a): Real induction arrows taken at 100 Hz frequency.
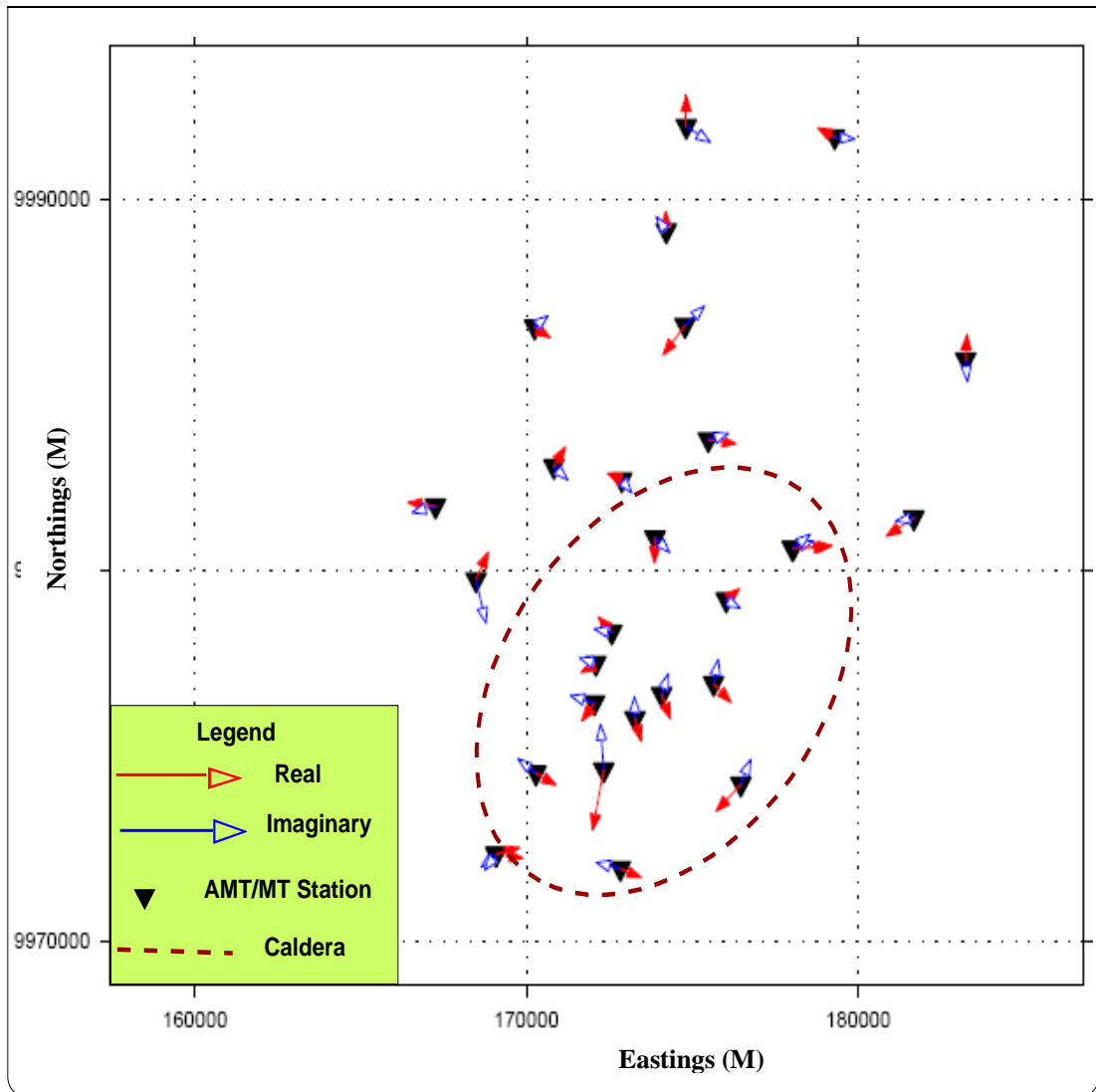
Figure 4.12 (b): Real induction arrows taken at 10 Hz frequency.
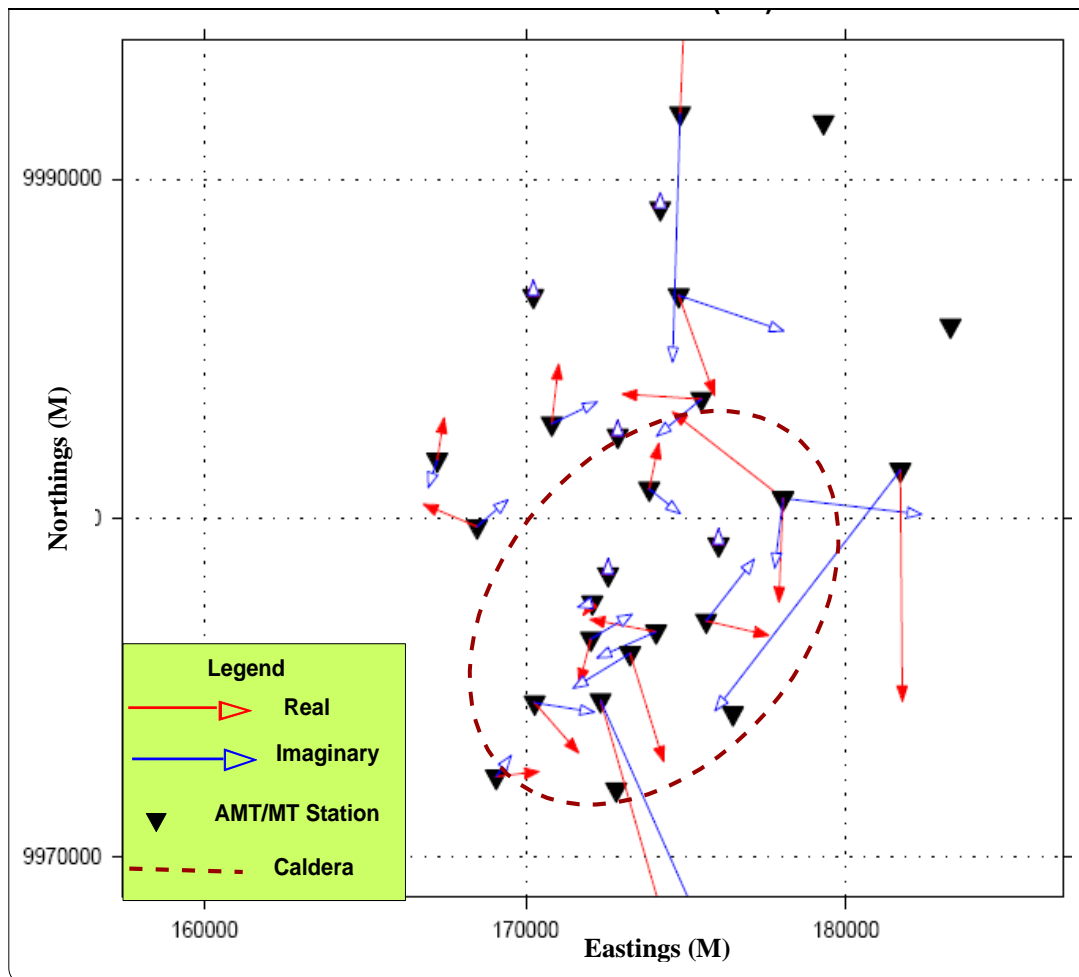
Figure 4.12 (c): Real induction arrows taken at 0.1 Hz frequency.

4.5 Impedance Ellipticity

The impedance ellipticity map taken at a period of 10s (Figure 4.13) at Menengai shows strong 2D to 3D effects below the caldera and along known structural features. This implies existence of a subsurface intrusion with 2D or 3D geometry. These effects are expected in geothermal areas associated with volcanic activity.
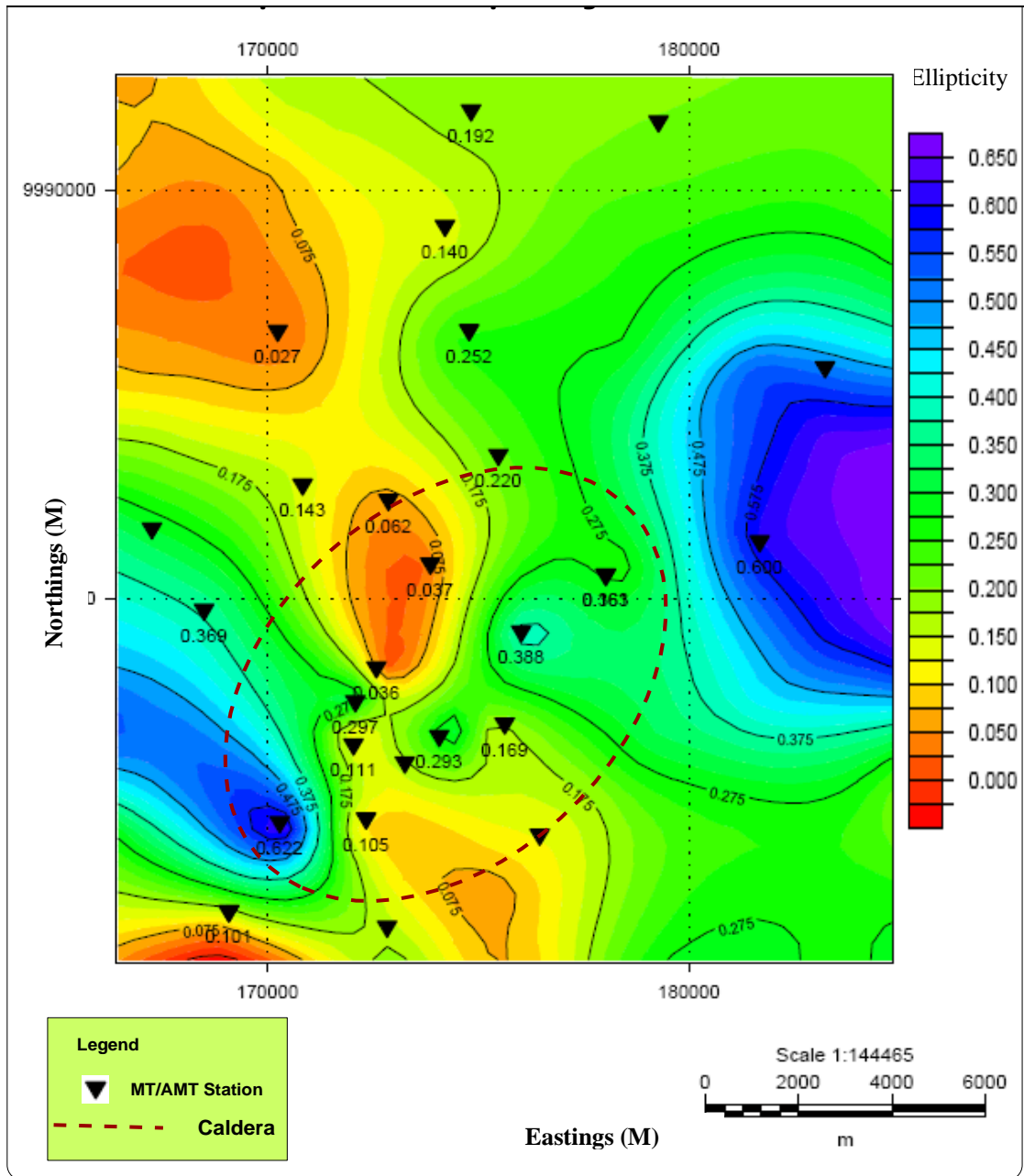
Figure 4.13: Impedance ellipticity map of the study area taken at 10s.

4.6 Resource Estimation

In Figure 5.3, the area under the 20 Ohm-m contour covers about half of the study area. Stacking anomalies recorded by the present study, it can be conclusively deduced that geothermal resources exist within the bounds of the large caldera. In estimating the extent of geothermal resources in this prospect, we take the area under the 20 Ohm-m contour that lie within the caldera.
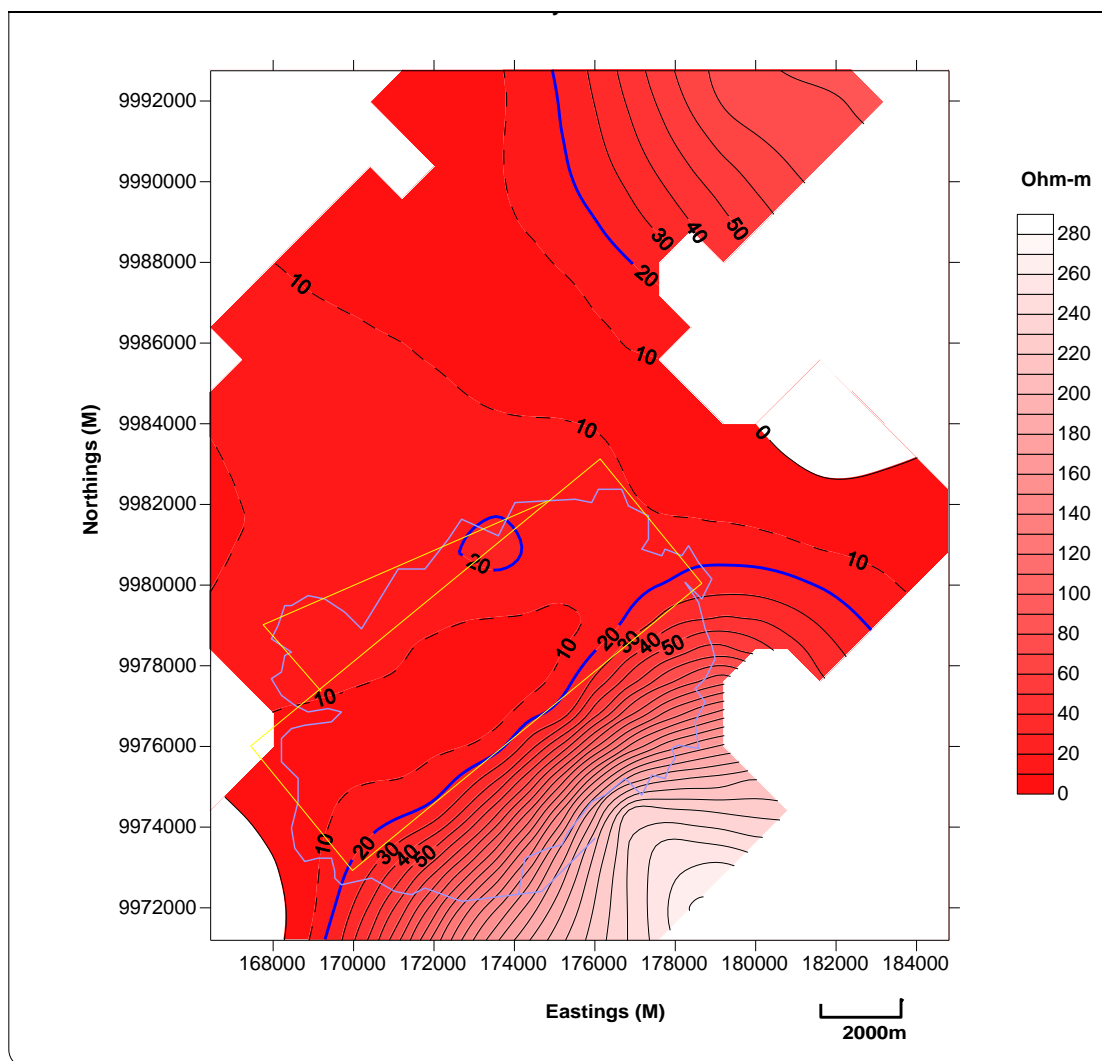
Figure 4.14: Areal extend of geothermal resources within Menengai caldera.

From figure 4.14 the estimated area within the caldera that is most prospective for geothermal resources may be calculated by taking the dimensions of the shown triangle and rectangle as shown in figure 4.15.
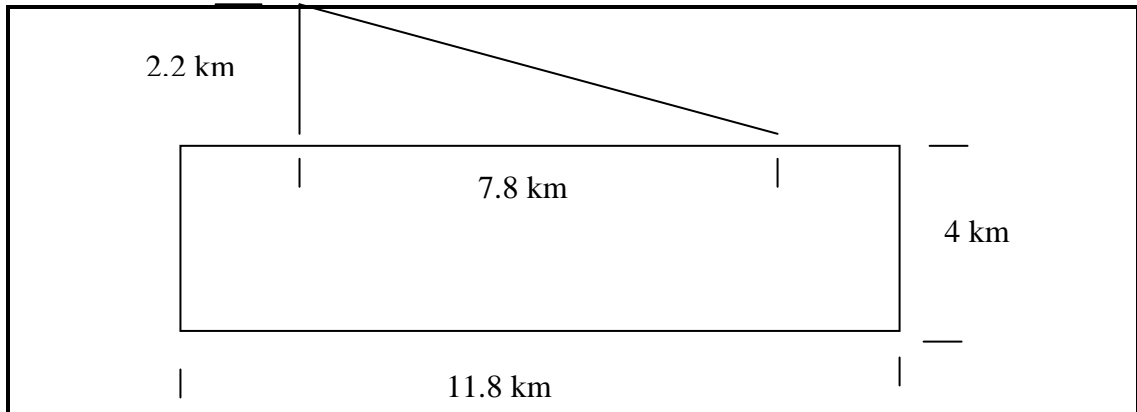
Figure 4.15: Estimation of area under 20 Ωm within the bounds of the Menengai Caldera

The Rectangle:

$Area_R = 11.8 \times 4 = 47.2 \text{ km}^2$

The Triangle:

$Area_T = \frac{1}{2} \times 7.8 \times 2.2 = 8.58 \text{ km}^2$

Therefore the total prospect area is $Area_R + Area_T$ which equals to;

$47.2 + 8.58 = \underline{55.78 \text{ km}^2}$

The estimated geothermal power potential for the Menengai area becomes;

Total area, A multiplied by the estimated generation capacity per unit area, Q;

55.78 km^2 x 15 MWe/km^2 = **836.7 MW** of electricity

CHAPTER FIVE

5.0 CONCLUSIONS AND RECOMMMENDATIONS

In this chapter deductions from the interpretation of resistivity data are presented. These results are used both to constrain the conceptual model for the geothermal field as well as in the estimation of a geothermal prospective area. This information is later used to estimate the electrical power generating potential of Menengai.

5.1 Resistivity

The interpretation of the integrated data set for Menengai concludes the following:

A geothermal system is shown to exist beneath the Menengai caldera. While there are indications that the resource extends outside the caldera, especially to the west and southern regions, the most part of the resource lies within the caldera.

The structural features in the area play a pivotal role in determining permeability in the prospect. The N-S trending fissure swarm associated with the rift meets with the two TVA at the centre of the caldera enhancing conductivity. A central conductive region is observed at this junction. The Solai TVA acts as a separator between the western caldera sector and the eastern region dominated by higher resistivity at most depths. The western, central and southern regions were found to be more conductive regions at shallow depths but are more resistive at depth.

It is shown that the anomalies exhibit multi-dimensional features at deeper depths. At shallower depths, the area is more homogeneous.

Below 2km depth, the three anomalies observed at the centre, western and southern caldera areas converge.

5.2 The Conceptual Model

This section compares the findings of the present study with those already reported by various other researchers regarding the components of the geothermal system. A conceptual model is also presented.

A dense body has been mapped by Simiyu and Keller (2001) using gravity. This body lies within 10 km depth below the caldera and extends southwards. The body has been found to attenuate seismic waves at shallow depth suggesting its composition to be partially molten magma. Most other intrusives in the area occur at shallow depths in the western half of the caldera, rather than to the east. Heat flow measured by KenGen (2004) found an average of 2690 MWt total heat flow within the caldera floor.

The present study confirms that a body with strong 2D and 3D characteristics exists at the central, western and southern caldera areas which tend to join together as one body at depths greater than 2 km and extends to great depth.

The setting of the prospect, at the rift floor, provides suitable conditions for its recharge from waters collected at either side of the rift flanks and percolating deeply through fissure swarms. Darling et al. (1995) inferred deep seated faults by suggesting a mantle source of CO_2 on the northwestern outskirts of the Menegai caldera. In the present study, areas of low resistivity are mapped directly below the

caldera walls and aligned with the fault system in the prospect area. These features appear to extend to greater depth.

Omenda (2000) observed that the primary permeability of volcanic materials found at Menengai and its environs varies from low to very low. To achieve good yield of steam reaching the surface a permeable subsurface media is essential. High Radon-222 and CO_2 counts are observed within the caldera floor with peak values observed towards the north and northwestern caldera walls. Fumaroles within the caldera show relatively high Rn/CO_2 ratio. These results were attributed by KenGen (2004) to hot magmatic bodies at temperatures not less than 250 °C. Extensional tectonics within the continental rift as well as intrusions as evidenced by high seismicity (Simiyu and Keller, 1997) also contributed to enhanced permeability in the region.

Evidence of vertical permeability in the present study is shown by increased conductivity along known structural features.

The Menengai and nearby eruptives centers comprise extensive pyroclastics containing a glassy halo crystalline component which is susceptible to hydrothermal alternation to yield hydrated clays (KenGen, 2004). It is inferred that this formation acts as the cap to the reservoir. The cap is mapped at the top of the reservoir as a shallow conductive signature that is relatively homogenous.

The findings above are used to develop a conceptual understanding of the prospect. In the pictorial model, an attempt is made to show the recharge, conduits and the heat sources. Based on interpreted outflows, we roughly approximate the 200°C

hypothetical temperature contour. The Conceptual models of the Menengai prospect are shown in Figures 5.1 and 5.2. The figures are not to scale.
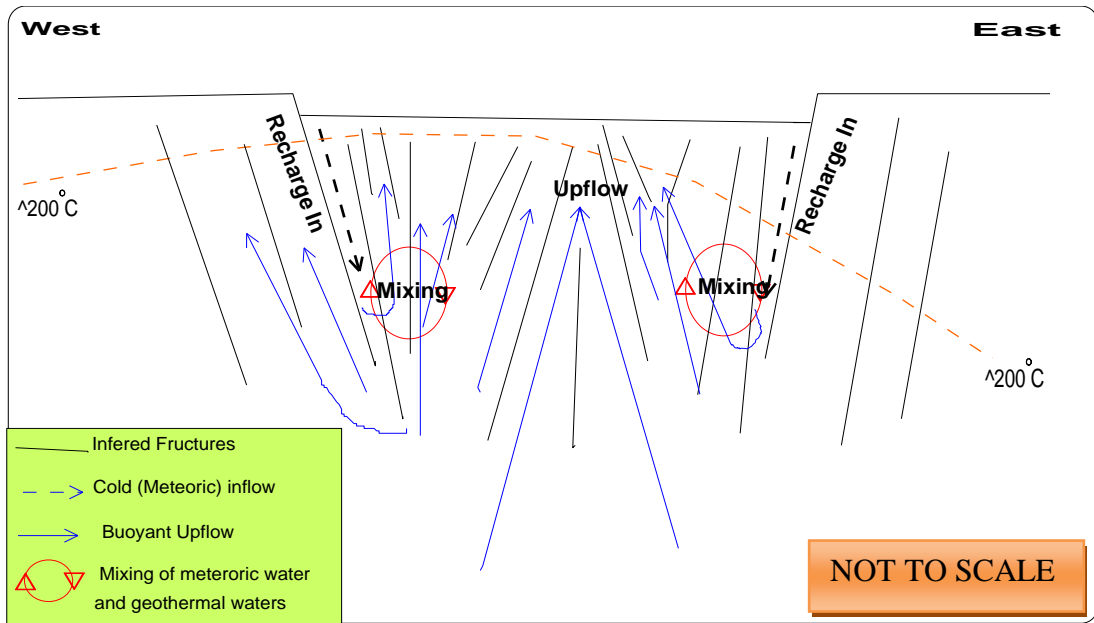
Figure 5.1: A Conceptual model along the E-W profile across Menengai caldera
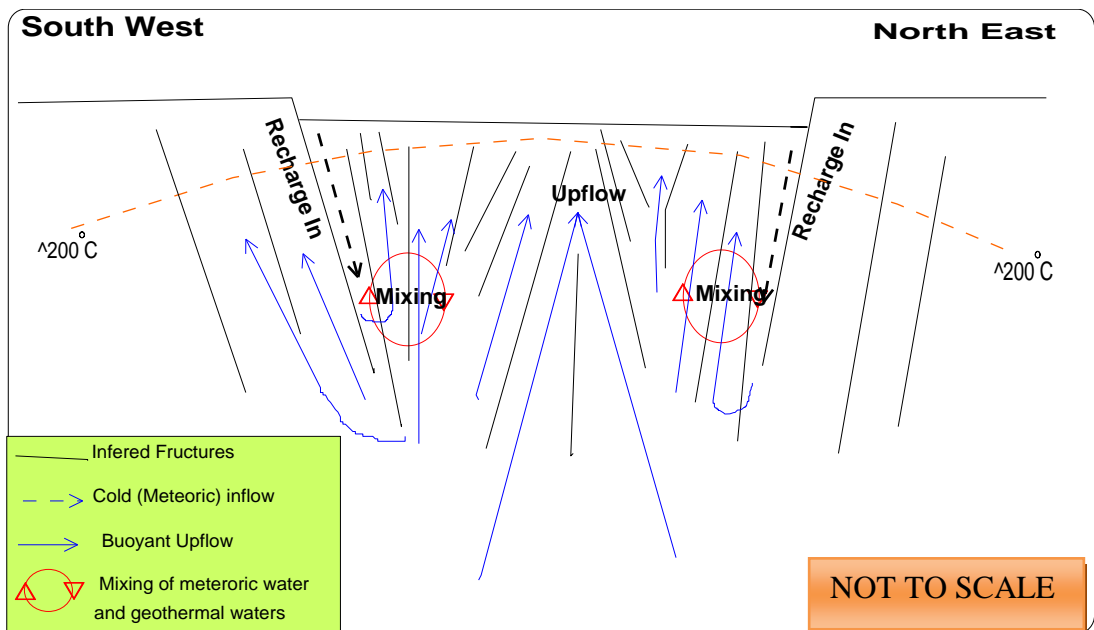
Figure 5.2: A Conceptual model of the prospect along the SW-NE profile.

5.3 Resource Estimation

The prospect is found to support the installation of a steam power generation plant similar to the one installed at Olkaria with capacity to produce at least 836 MW of steady electricity production for 25 years.

5.4 Recommendations for future work

Four recommendations were made for further work. Firstly, future work is recommended to study the anomaly located at Olrongai area and the possibility of there being a connection to the one observed beneath the Menengai caldera. Secondly, there is need to collect more data towards the east of the caldera to study a possible reservoir beneath the eastern caldera wall. The other recommendation is to investigate deep seated low resistivity signatures on either side of the postulated reservoir. Finally, there is need to accurately determine temperature contours, outflow and inflow zones by using down-hole temperature logs.

LIST OF PUBLICATIONS

Saitet, D., 2010: Integrated Resistivity Imaging of the Suswa Geothermal Field-Kenya, Saint Petersburg, Russia, 2010, European Association of Geoscientists and Engineers conference paper C20E.

Saitet, D., 2010a: Static shift effects on wide range Magnetotellurics in the Kenyan central rift geothermal system, Presented at the Faculty of Science, Postgraduate Seminar 2010, JKUAT.

REFERENCES

A'rnason, K., 1989: Central loop transient electromagnetic sounding over a horizontal layered earth. Orkustofnun, Reykjavik, report OS-89032/JHD-06, 129pp.

Bertani R, 2005: World geothermal power generation in the period 2001–2005, *Geothermics*, 2005; **34**:651–90.

Cagniard, L., 1953: Basic theory of the Magnetotelluric method: *Geophysics, V. 18, No.3, 605-635pp*

Fox, L., 2003: Past, Present and Future of Magnetotellurics. Presentation to the KEGS 50th Aniversary Conference, Toronto, Canada.

Geotermica Italiana, 1987: Geothermal Reconaissance Survey in the Menengai-Bogoria area of the Kenya Rift Valley. Final Report.

Ingerov, O.I, Fox, L., Golyashov, A., and Colin, A., 2009: P251 Non-grounded Surface Electroprospecting Technique. Extended Abstract. 71st EAGE Conference and Exhibition-Amsterdam, The Netherlands, 8-11 June 2009.

Jones, A.G., 1988: Static shift of magnetotelluric data and its removal in a sedimentary basin environment. *Geophysics*, **53-7:** 967-978.

Kaufman, A. A and Keller G.V., 1983: Frequency and Transient soundings. Elsevier N.Y

Kiva, I.N, 2009: GOK responses to the energy crisis.Presented during the experts roundtable on the current crisis in Kenya on 27th August, 2009.

KenGen, 2004: Menengai Volcano: Investigations for its geothermal potential-a geothermal resource assessment project.

KenGen, 2008: Water resources assessment for drilling in the Menengai geothermal prospect, Kenya. A report compiled by Dr. Stephen Onacha.

Kenya Gazette, 2009: Gazette notice no.6065, National task force on accelerated development of green energy, June 2009

Marcus, G, 1999: Magnetic distortion of GDS transfer functions: An example from the Penninic Alps of Eastern Switzerland revealing a crustal conductor, *Earth Planets Space*, **51**: 1023–1034, 1999

Mariita, N.O., 2003: An integrated geophysical study of the northern Kenya rift crustal structure: implications for geothermal energy prospecting for Menengai area. *A PhD dissertation, University of Texas at El Paso, USA*.

McCall, G.J.H, 1967: Geology of the Nakuru-Thomson's Falls-Lake Hannington Area, Degree Sheet No. 35 SW and 43 NW Quarter.

Ofwona, C., 2008: Geothermal Resource Assesment-Case Example Olkaria 1, Presented at Short Course III on Exploration for Geothermal Resources, Organized by UNU- GTP and KenGen at Lake Naivasha, Kenya, October 24- November 17, 2008.

Omenda, P., 2000: Anatectic origin for Comendite in Olkaria geothermal field, Kenya Rift; Geochemical evidence for syenitic protholith. *African Journal of Sciences and Technology. Science and Engineering series,* **1:** 39-47.

Pullerin, L., Hohmann, G.W., 1990: Transient Electromagnetic Inversion: A remedy for Magnetotelluric static shifts: *Geophysics,* **55:**1242-1250.

Ranganayaki, **R.P, 1984:** An Interpretive Analysis of Magnetotelluric data: *Geophysics,* **49:** 1730-48.

Rokityansky, I.I., 1982: Geoelectromagnetic Investigation of the Earth's Crust and Mantle. Springer-Verlag, Berlin, Heidelberg, New York, 378pp.

Schumucker, U., 1970: Anomalies of the magnetic variations in the southwestern United States, Bull. Scripps Inst. Oceanogr., 13, University of California Press.

Simiyu, S.M., 1996. Integrated geophysical study of the crustal structure of the southern Kenya Rift. *A PhD Dissertation, University Texas El Paso, USA*

Simiyu, S. M., and Keller, G. R., 1997: Integrated geophysical analysis of the East African Plateau from gravity anomalies and recent seismic studies. *Tectonophysics,* **278**:291-314.

Simiyu, S. M., and Keller, G. R., 2001: An Integrated geophysical analysis of the upper crust of the southern Kenya rift, *International Journal of Geophysics*, **147**: 543-561.

Simpson, F., and Bahr, K., 1956: Practical magnetotellurics. Cambridge University Press, Cambridge; New York, 2005

Sternberg, B. K., Washbourne, J.C., Pullerin, L., 1988: Correction for the static shift in Magnetotellurics using Transient Electromagnetic soundings. *Geophysics,* **53**:1459-1468.

UNU-GTP/KenGen, 2008: Short Course III on Exploration for Geothermal resources organized by UNU-GTP and KenGen, in Naivasha, Kenya, 24 October- 17 November, 2008. Editors: L. S Georgsson, D.H Holm, S.M Simiyu and N. Mariita.

Ward, S.H, and Wannamaker, P.E., 1983: The MT/AMT electromagnetic method in geothermal exploration, UNU-GTP, Iceland, report 5, 107 pp.

APPENDICES

This section presents four sets of data from established stations at Menengai that demonstrate the process of data analysis covering raw cross powers, raw station data to 1dimensional inversions that give rise to the iso-resistivity maps presented earlier in chapter four.

Appendix I: Raw data showing the apparent resistivity and phase versus frequency for Station MENMT101.
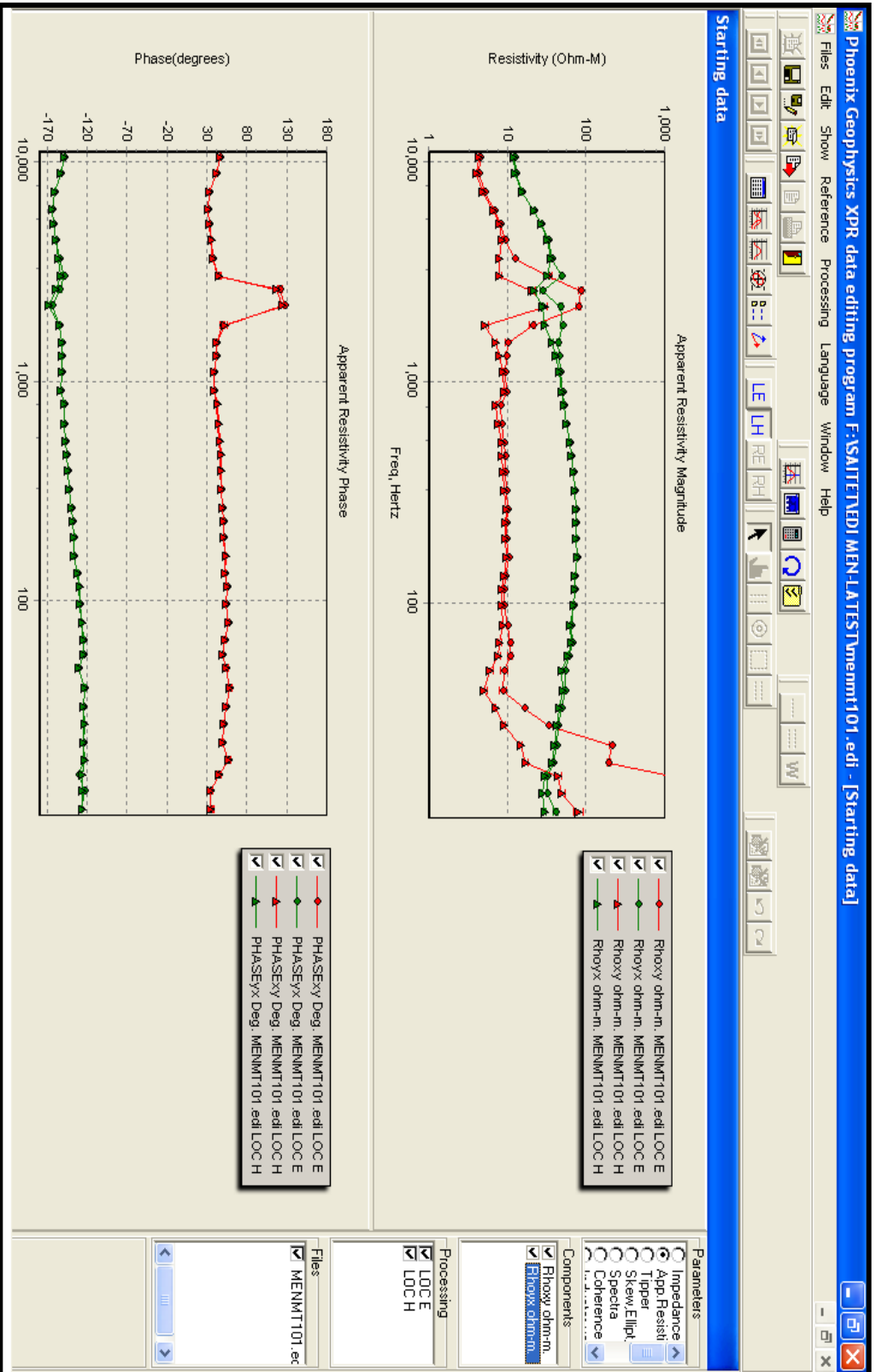
Appendix II: 1-D inversion of MT data from station MENAMT86
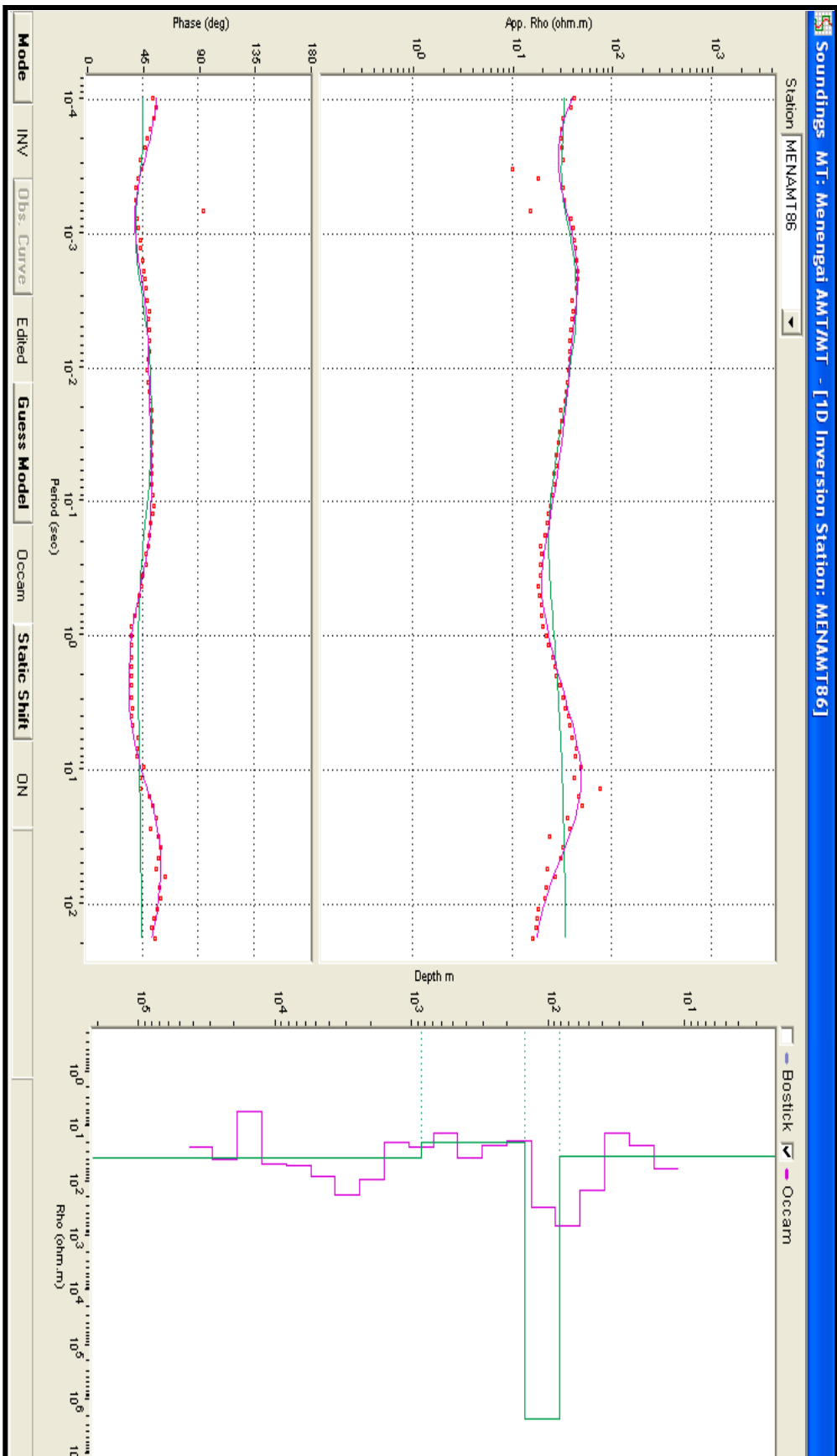
APPENDIX III: MENMT 101 DATA SET

RUN INFORMATION   STATION 1

PROCESSED FROM DFT TIME SERIES   STN Number: MENM08-T101

 SURVEY: MENEMT   Site Desc; BadR: 0 SatR: 0

COMPANY: kengen   Lat 00:15:111S Long 036:03:401E

 JOB: MEN   Elevation: 2154   Meters.

Reference Site: MENMT101

HARDWARE: MTU5A   Site Permitted by: MOE

START-UP: 2008/10/01 - 06:00:00   Site Layout by: ELVIS

END-TIME: 2008/12/21 - 12:42:10   SYSTEM INFORMATION

FILE: 1973C21A   MTU-Box Serial Number: U-1973

MTUPROG VERSION: 3112F6   MTU-Box Gains:E`s x 4 H`s x 4

MTU-DFT VERSION: TStoFT.31   MTU-Ref Serial Number: U-1973

MTU-RBS VERSION:R2007-1127-B18   Comp Chan#   Sensor   Azimuth

Reference Field: Local H - Ref.   Ex1   1   60.00 M   0.0 DGmn

 XPR Weighting: RHO Variance.   Ey1   2   60.00 M   90.0 DGmn

RBS: 1 COH: 0.85 RHO VAR: 0.75   Hx1   3   AMT1639   0.0 DGmn

73

CUTOFF: 0.00 COH: 35 % VAR: 25 %   Hy1   4   AMT1641   90.0 DGmn

Notch Filters set for 50 Hz.   Hz1   5   AMT1644

                          RHx3   6   AMT1639   0.0 DGmn

 Comp   MTU box S/N Temp   RHy3   7   AMT1641   90.0 DGmn

Ex & Ey: MTU5A   1973   44 C   Ebat:12.6V Hbat:12.6V Rbat:12.6V

Hx & Hy: MTU5A   1973   44 C   Ex Pot Resist: 0.100 Kohms

  Hz: MTU5A   1973   44 C   Ex Voltage:AC=10.8mV, DC=+1240mV

Rx & Ry: MTU5A   1973   44 C   Ey Pot Resist: 0.100 Kohms

 Hx Sen: AMT1639   Ey Voltage:AC=19.6mV, DC=+1210mV

 Hy Sen: AMT1641

 Hz Sen: AMT1644

 Rx Sen:

 Ry Sen:

Read Oplog lines MENMT101.MMT

OPLG-TIME: MENM08-T101Hx1 SHy1 SHz1 SHx1 SHy1

RegTime   =21/12/08 12:21:00 PM

EndRegTime=21/12/08 12:42:00 PM

C:\MenMT\MENMT101.EMT Loc H

C:\MenMT\MENMT101.MMT Loc H

Frequency grid, Hz:, Number=40(40) C:\MenMT\MENMT101.EMT

 110400.0000000 2 8800.0000000 3 7200.0000000 4 6000.0000000 5 5200.00000
00

 6 4400.0000000 7 3600.0000000 8 3000.0000000 9 2600.0000000 10 2200.00000
00

 11 1800.0000000 12 1500.0000000 13 1300.0000000 14 1100.0000000 15 900.000
0000

 16 780.0000000 17 640.0000000 18 530.0000000 19 460.0000000 20 390.00000
00

 21 320.0000000 22 265.0000000 23 229.0000000 24 194.0000000 25 159.00000
00

 26 132.0000000 27 115.0000000 28   97.0000000 29   79.0000000 30   66.0000000

 31   57.0000000 32   49.0000000 33   40.0000000 34   33.0000000 35   27.5000000

 36   22.5000000 37   18.8000000 38   16.2000000 39   13.7000000 40   11.2000000

Edit plot number: 0

Frequency grid, Hz:, Number=40(40) C:\MenMT\MENMT101.MMT

1 320.0000000 2 265.0000000 3 229.0000000 4 194.0000000 5 159.0000000

6 132.0000000 7 115.0000000 8 97.0000000 9 79.0000000 10 66.0000000

11 57.0000000 12 49.0000000 13 40.0000000 14 33.0000000 15 27.5000000

16 22.5000000 17 18.8000000 18 16.2000000 19 13.7000000 20 11.2000000

21 9.4000000 22 8.1000000 23 6.9000000 24 5.6000000 25 4.7000000

26 4.1000000 27 3.4000000 28 2.8100000 29 2.3400000 30 2.0300000

31 1.7200000 32 1.4100000 33 1.1700000 34 1.0200000 35 0.8600000

36 0.7000000 37 0.5900000 38 0.5100000 39 0.4300000 40 0.3500000

Edit plot number: 0

New frequency grid, Hz:, Number=60

 110400.0000000 2 8800.0000000 3 7200.0000000 4 6000.0000000 5 5200.00000
00

 6 4400.0000000 7 3600.0000000 8 3000.0000000 9 2600.0000000 10 2200.00000
00

11 1800.0000000 12 1500.0000000 13 1300.0000000 14 1100.0000000 15 900.000
0000

16 780.0000000 17 640.0000000 18 530.0000000 19 460.0000000 20 390.00000
00

21 320.0000000 22 265.0000000 23 229.0000000 24 194.0000000 25 159.00000

00

26 132.0000000 27 115.0000000 28 97.0000000 29 79.0000000 30 66.0000000

31 57.0000000 32 49.0000000 33 40.0000000 34 33.0000000 35 27.5000000

36 22.5000000 37 18.8000000 38 16.2000000 39 13.7000000 40 11.2000000

41 9.4000000 42 8.1000000 43 6.9000000 44 5.6000000 45 4.7000000

46 4.1000000 47 3.4000000 48 2.8100000 49 2.3400000 50 2.0300000

51 1.7200000 52 1.4100000 53 1.1700000 54 1.0200000 55 0.8600000

56 0.7000000 57 0.5900000 58 0.5100000 59 0.4300000 60 0.3500000

XPRS number in Input MT-files

1	20	2	20	3	20	4	20	5	20
6	20	7	20	8	20	9	20	10	20
11	20	12	20	13	20	14	20	15	20
16	20	17	20	18	20	19	20	20	20
21	40	22	40	23	40	24	40	25	40
26	40	27	40	28	40	29	40	30	40
31	40	32	40	33	40	34	40	35	40

36	40	37	40	38	40	39	40	40	40
41	20	42	20	43	20	44	20	45	20
46	20	47	20	48	20	49	20	50	20
51	20	52	20	53	20	54	20	55	20
56	20	57	20	58	20	59	20	60	20

XPRS number in Summed MT-File

1	20	2	20	3	20	4	20	5	20
6	20	7	20	8	20	9	20	10	20
11	20	12	20	13	20	14	20	15	20
16	20	17	20	18	20	19	20	20	20
21	40	22	40	23	40	24	40	25	40
26	40	27	40	28	40	29	40	30	40
31	40	32	40	33	40	34	40	35	40
36	40	37	40	38	40	39	40	40	40
41	20	42	20	43	20	44	20	45	20
46	20	47	20	48	20	49	20	50	20
51	20	52	20	53	20	54	20	55	20

56　　　20 57　　　20 58　　　20 59　　　20 60　　　20

APPENDIX IV: MENAMT86 DATA SET

RUN INFORMATION   STATION 1

PROCESSED FROM DFT TIME SERIES   STN Number: MENM08-T86

SURVEY: DOMES MT   Site Desc; BadR: 0 SatR: 26

COMPANY: KENGEN   Lat 00:09:193S Long 036:02:354E

JOB: MEN   Elevation: 1980   Meters.

Reference Site: MENAMT86

HARDWARE: MTU5A   Site Permitted by:

START-UP: 2008/10/01 - 06:00:00   Site Layout by: TOM

END-TIME: 2008/12/18 - 06:28:40   SYSTEM INFORMATION

FILE: 2194C17C   MTU-Box Serial Number: U-2194

MTUPROG VERSION: 3112F6   MTU-Box Gains:E`s x 4 H`s x 4

MTU-DFT VERSION: TStoFT.31   MTU-Ref Serial Number: U-2194

MTU-RBS VERSION:R2007-1127-B18   Comp Chan#   Sensor   Azimuth

Reference Field: Local H - Ref.   Ex1   1   60.00 M   0.0 DGmn

 XPR Weighting: RHO Variance.   Ey1   2   60.00 M   90.0 DGmn

RBS: 1 COH: 0.95 RHO VAR: 0.95   Hx1   3   COIL2483   0.0 DGmn

80

CUTOFF: 0.00 COH: 75 % VAR: 75 %   Hy1   4   COIL2486   90.0 DGmn

Notch Filters set for 50 Hz.   Hz1   5   COIL2490

                              RHx3   6   COIL2483   0.0 DGmn

 Comp   MTU box S/N Temp   RHy3   7   COIL2486   90.0 DGmn

Ex & Ey: MTU5A   2194   48 C   Ebat:12.1V Hbat:12.1V Rbat:12.1V

Hx & Hy: MTU5A   2194   48 C   Ex Pot Resist: 0.390 Kohms

   Hz: MTU5A   2194   48 C   Ex Voltage:AC=3.59mV, DC=+1.10mV

Rx & Ry: MTU5A   2194   48 C   Ey Pot Resist: 0.324 Kohms

 Hx Sen: COIL2483   Ey Voltage:AC=24.4mV, DC=+4.90mV

 Hy Sen: COIL2486

 Hz Sen: COIL2490

 Rx Sen:

 Ry Sen:

Read Oplog lines MENMT86.MTL

OPLG-TIME: MENM08-T86 Hx1 SHy1 SHz1 SHx1 SHy1

RegTime   =18/12/08 5:59:00 AM

EndRegTime=18/12/08 6:28:00 AM

C:\MenMT\MENMT86.MTH Loc H

C:\MenMT\MENMT86.MTL Loc H

Frequency grid, Hz:, Number=40(40) C:\MenMT\MENMT86.MTH

 1 320.0000000 2 265.0000000 3 229.0000000 4 194.0000000 5 159.0000000

 6 132.0000000 7 115.0000000 8 97.0000000 9 79.0000000 10 66.0000000

11 57.0000000 12 49.0000000 13 40.0000000 14 33.0000000 15 27.5000000

16 22.5000000 17 18.8000000 18 16.2000000 19 13.7000000 20 11.2000000

21 9.4000000 22 8.1000000 23 6.9000000 24 5.6000000 25 4.7000000

26 4.1000000 27 3.4000000 28 2.8100000 29 2.3400000 30 2.0300000

31 1.7200000 32 1.4100000 33 1.1700000 34 1.0200000 35 0.8600000

36 0.7000000 37 0.5900000 38 0.5100000 39 0.4300000 40 0.3500000

Edit plot number: 0

Frequency grid, Hz:, Number=40(40) C:\MenMT\MENMT86.MTL

 1 0.2930000 2 0.2540000 3 0.2150000 4 0.1760000 5 0.1460000

 6 0.1270000 7 0.1070000 8 0.0880000 9 0.0730000 10 0.0630000

11 0.0540000 12 0.0440000 13 0.0370000 14 0.0320000 15 0.0269000

16 0.0220000 17 0.0183000 18 0.0159000 19 0.0134000 20 0.0110000

21 0.0092000 22 0.0079000 23 0.0067000 24 0.0055000 25 0.0046000

26 0.0040000 27 0.0034000 28 0.0027500 29 0.0022900 30 0.0019800

31 0.0016800 32 0.0013700 33 0.0011400 34 0.0009900 35 0.0008400

36 0.0006900 37 0.0005700 38 0.0005000 39 0.0004200 40 0.0003400

Edit plot number: 0

New frequency grid, Hz:, Number=80

 1 320.0000000 2 265.0000000 3 229.0000000 4 194.0000000 5 159.0000000

 6 132.0000000 7 115.0000000 8 97.0000000 9 79.0000000 10 66.0000000

11 57.0000000 12 49.0000000 13 40.0000000 14 33.0000000 15 27.5000000

16 22.5000000 17 18.8000000 18 16.2000000 19 13.7000000 20 11.2000000

21 9.4000000 22 8.1000000 23 6.9000000 24 5.6000000 25 4.7000000

26 4.1000000 27 3.4000000 28 2.8100000 29 2.3400000 30 2.0300000

31 1.7200000 32 1.4100000 33 1.1700000 34 1.0200000 35 0.8600000

36 0.7000000 37 0.5900000 38 0.5100000 39 0.4300000 40 0.3500000

41 0.2930000 42 0.2540000 43 0.2150000 44 0.1760000 45 0.1460000

46 0.1270000 47 0.1070000 48 0.0880000 49 0.0730000 50 0.0630000

51 0.0540000 52 0.0440000 53 0.0370000 54 0.0320000 55 0.0269000

56   0.0220000 57   0.0183000 58   0.0159000 59   0.0134000 60   0.0110000

61   0.0092000 62   0.0079000 63   0.0067000 64   0.0055000 65   0.0046000

66   0.0040000 67   0.0034000 68   0.0027500 69   0.0022900 70   0.0019800

71   0.0016800 72   0.0013700 73   0.0011400 74   0.0009900 75   0.0008400

76   0.0006900 77   0.0005700 78   0.0005000 79   0.0004200 80   0.0003400

XPRS number in Input MT-files

1	20	2	20	3	20	4	20	5	20
6	20	7	20	8	20	9	20	10	20
11	20	12	20	13	20	14	20	15	20
16	20	17	20	18	20	19	20	20	20
21	20	22	20	23	20	24	20	25	20
26	20	27	20	28	20	29	20	30	20
31	20	32	20	33	20	34	20	35	20
36	20	37	20	38	20	39	20	40	20
41	20	42	20	43	20	44	20	45	20
46	20	47	20	48	20	49	20	50	20
51	20	52	20	53	20	54	20	55	20

| 56 | 20 57 | 20 58 | 20 59 | 20 60 | 20 |

| 61 | 20 62 | 20 63 | 20 64 | 20 65 | 20 |

| 66 | 20 67 | 20 68 | 20 69 | 20 70 | 20 |

| 71 | 20 72 | 20 73 | 20 74 | 20 75 | 20 |

| 76 | 20 77 | 20 78 | 20 79 | 20 80 | 20 |

XPRS number in Summed MT-File

| 1 | 20 2 | 20 3 | 20 4 | 20 5 | 20 |

| 6 | 20 7 | 20 8 | 20 9 | 20 10 | 20 |

| 11 | 20 12 | 20 13 | 20 14 | 20 15 | 20 |

| 16 | 20 17 | 20 18 | 20 19 | 20 20 | 20 |

| 21 | 20 22 | 20 23 | 20 24 | 20 25 | 20 |

| 26 | 20 27 | 20 28 | 20 29 | 20 30 | 20 |

| 31 | 20 32 | 20 33 | 20 34 | 20 35 | 20 |

| 36 | 20 37 | 20 38 | 20 39 | 20 40 | 20 |

| 41 | 20 42 | 20 43 | 20 44 | 20 45 | 20 |

| 46 | 20 47 | 20 48 | 20 49 | 20 50 | 20 |

| 51 | 20 52 | 20 53 | 20 54 | 20 55 | 20 |

56	20	57	20	58	20	59	20	60	20
61	20	62	20	63	20	64	20	65	20
66	20	67	20	68	20	69	20	70	20
71	20	72	20	73	20	74	20	75	20
76	20	77	20	78	20	79	20	80	20